ACS APPLIED MATERIALS & INTERFACES

www.acsami.org
Research Article

Stem Cells from Human Exfoliated Deciduous Teeth-Derived Exosomes for the Treatment of Acute Liver Injury and Liver Fibrosis

Ziyuan Wang,[#] Danyang Zhong,[#] Tingting Yan,[#] Qiang Zheng, Enjie Zhou, Zhichao Ye, Xiaoyan He, Yu Liu, Jianing Yan, Yuyang Yuan, Yifan Wang,[*] and Xiujun Cai[*]

Cite This: *ACS Appl. Mater. Interfaces* 2025, 17, 17948−17964

Read Online

ACCESS | Metrics & More | Article Recommendations | Supporting Information

ABSTRACT: Mesenchymal stem cells (MSCs) play a crucial role in regenerative medicine due to their regenerative potential. However, traditional MSC-based therapies are hindered by issues such as microvascular obstruction and low cell survival after transplantation. Exosomes derived from MSCs (MSC-Exo) provide a cell-free, nanoscale alternative, mitigating these risks and offering therapeutic potential for liver diseases. Nonetheless, the functional variability of MSCs from different sources complicates their clinical application. Stem cells derived from human exfoliated deciduous teeth (SHED) offer advantages such as ease of procurement and robust proliferative capacity, but their secretome, particularly SHED-Exo, remains underexplored in the context of liver disease therapy. This study analyzed MSC-Exo from various sources via small RNA sequencing to identify differences in microRNA profiles, aiding in the selection of optimal MSC sources for clinical use. SHED-Exo was subsequently tested in an acute liver injury model, showing notable regenerative effects, including enhanced hepatocyte proliferation, macrophage polarization, and reduced inflammation. Despite strong liver-targeting properties, the rapid hepatic clearance of SHED-Exo limits its effectiveness in chronic liver diseases. To address this challenge, a GelMA-based hydrogel was developed for in situ delivery, ensuring sustained release and enhanced antifibrotic efficacy, providing a promising strategy for chronic liver disease management.

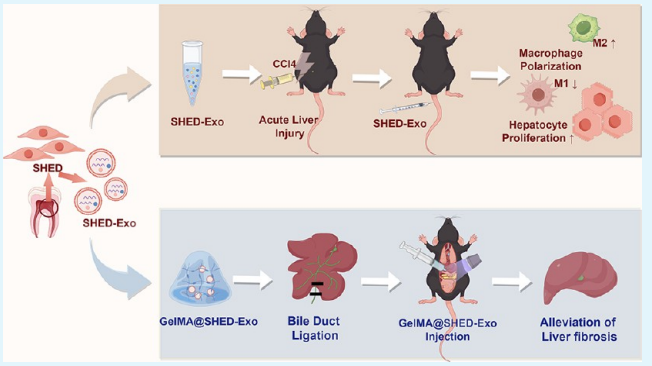

KEYWORDS: *liver regeneration, exosome, hydrogel, liver fibrosis, mesenchymal stem cell*

INTRODUCTION

As life expectancy increases, liver diseases have emerged as a significant global health concern and economic burden due to their high incidence and mortality rates.[1,2] Many liver conditions remain inadequately treated, often advancing to end-stage liver disease, where patients must wait for liver transplants. This challenge has spurred interest in regenerative medicine and tissue engineering as alternative therapeutic strategies.[3,4] Mesenchymal stem cell (MSC)-based therapies are particularly promising in this field, owing to MSCs' abilities for self-renewal and differentiation into diverse cell lineages. MSCs can be derived from various adult tissues, including bone marrow, adipose tissue, umbilical cord, amniotic fluid, and dental pulp, with their biological effects varying according to the source.[5−7] Oral MSCs are a more recent focus compared to extensively studied sources, such as umbilical cord MSCs (UC-MSCs) and adipose-derived MSCs (ADSCs). While research on oral MSCs is still emerging and comparative studies are limited, these cells offer distinct advantages, such as minimally invasive and safe harvesting procedures and enhanced biological activity. Studies indicate that oral MSCs play a crucial role in tissue engineering and regenerative repair.[8] Several types of oral stem cells have been identified, including stem cells from human exfoliated deciduous teeth (SHED), dental pulp stem cells, and gingival MSCs.[9,10] Among these, SHED represent a readily accessible and minimally invasive source of MSCs, as they are naturally shed during childhood.[11−15] This characteristic provides a plentiful and ethically noncontroversial means of harvesting. In comparison to other MSC sources, such as bone marrow, adipose tissue, and umbilical cord, SHED offer several advantages, including minimal ethical concerns, ease of collection, minimal invasiveness, safety, and the potential for self-renewal.[11] SHED also maintain high stem cell potential, encompassing cell proliferation, pluripotency, and immune regulatory functions.[15] These attributes render SHED a promising

Received: November 15, 2024
Revised: March 6, 2025
Accepted: March 6, 2025
Published: March 14, 2025

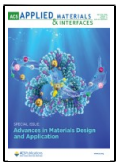

Scheme 1. Study Workflow[a]

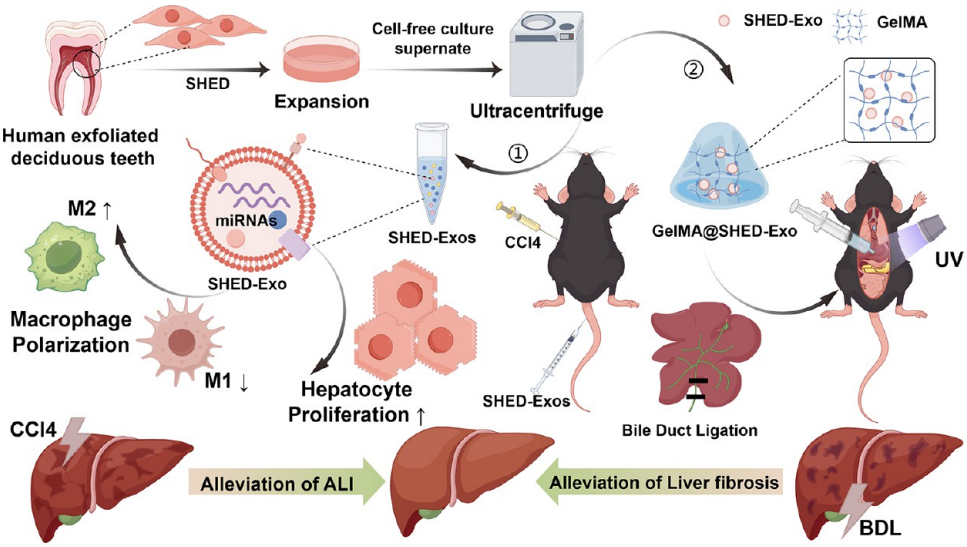

[a]SHED-exo and GelMA@SHED-exo preparation. Schematic representation of the expected effect of SHED-exo in acute liver injury and liver fibrosis (the figure was generated with Figdraw).

candidate for regenerative therapies aimed at liver diseases, tissue repair, and immunomodulation.

The liver plays essential roles in digestion, detoxification, and metabolism, and its dysfunction can lead to serious conditions, such as ALI and chronic liver diseases like fibrosis. Given the complexities of treating these conditions, new therapeutic strategies are needed. Due to the complex mechanism, numerous challenges persist in the treatment and prevention of liver injury.[16] Extensive research has demonstrated the effectiveness of stem cell therapies in addressing these pathological changes, particularly with MSCs in treating liver injury. Many of these studies have advanced to clinical trials.[17] Unlike treatments for acute conditions such as ALI, chronic liver diseases often require prolonged and repeated cell infusions, which increases the associated risks of cell transplantation. Considering the limitations of efficacy and side effects of the aforementioned liver-protecting drugs, novel stem cell-based cell therapies have emerged as a promising new strategy for tissue repair.[18]

In recent years, considerable emphasis has been placed on the prospective application of MSC-derived exosomes to enhance the management of inflammatory and degenerative conditions due to their immunomodulatory properties.[19] Exosomes are a class of diminutive lipid membrane vesicles (30−150 nm) whose biological function is often determined by the secreting cell of origin.[20] Exosomes actively participate in various cellular interactions, including information transfer, antigen presentation, immune and target cell regulation, and tissue regeneration, by transporting cellular proteins, nucleic acids, lipids, and metabolites.[21] Several studies have highlighted the enhanced efficacy of MSCs and its derived exosomes on liver injury,[18] underscoring significant potential for the application of MSC-derived exosomes in ALI therapeutics. Recent investigations have shown a preference for exploring the potential of exosomes derived from bone marrow mesenchymal stem cells (BMSCs) or umbilical cord-derived MSCs in liver regeneration or attenuation of liver fibrosis following hepatectomy.[22] However, research on the use of oral-derived MSCs for treating liver diseases remains limited.[23] For instance, only a few studies have explored the therapeutic potential of SHED for liver conditions such as fibrosis, acute liver failure, and nonalcoholic steatohepatitis,[24−26] with only one study indicating that SHED's secretome may have antifibrotic effects.[27] No studies have yet investigated the use of SHED-derived exosomes (SHED-Exo) for liver disease treatment. To address this gap, this study focuses on SHED-Exo as the primary research subject. Initially, sRNA sequencing was conducted to analyze the shared and unique microRNAs (miRNAs) carried by exosomes from three different MSC sources, providing a preliminary assessment of SHED-Exo's therapeutic potential. Subsequently, SHED-Exo was applied to an ALI model to evaluate its efficacy in mitigating damage, reducing inflammation, and promoting regeneration. Finally, to enhance SHED-Exo's impact on liver fibrosis, a novel hydrogel-based delivery system was developed to prolong SHED-Exo's retention in liver tissue, enabling targeted and sustained release (Scheme 1).

MATERIALS AND METHODS

Animal Ethics. The Laboratory Animal Welfare and Ethics Committee of Zhejiang University approved all animal experimental procedures used in this study in concordance with the NIH guidelines for the care and use of laboratory animals.

Animals and Treatment. All animal experiments applied in the following were conducted after approval of the Ethical Review Committee for Laboratory Animals of Zhejiang University. C57BL/6 mice (weighing 18−22 g, male, 7 weeks old) were purchased from the experimental Animal Center of Zhejiang University. After arriving at the Animal Experiment Center, mice were quarantined and adapted to the culture environment for 1 week before experiments were carried out. During the animal rearing period, the animals were independently ventilated according to the SPF-grade rearing standard, given standard food and water, and alternated with light/dark for 12 h.

Cell Lines and Cell Culture. ADSCs, UC-MSCs, and SHED were purchased from Exosomic Biomed Ltd. ADSCs were cultured in complete Dulbecco's modified Eagle's medium (DMEM, Gibco, USA), supplemented with 10% fetal bovine serum (FBS, Gibco, USA) and 1% penicillin/streptomycin (Gibco, USA). ADSCs were grown at an initial density of 3×10^5 cells on T75 flasks and maintained at 37 °C in 90% humidified air with 5% CO_2. The medium was replaced

https://doi.org/10.1021/acsami.4c19748
ACS Appl. Mater. Interfaces 2025, 17, 17948−17964

every third day.[28] When 80% confluency was reached, cells were detached using 0.25% Trypsin-EDTA (Gibco, USA) for the experiments.

UC-MSCs were cultured at 37 °C in a humidified atmosphere of 5% CO_2 in a serum-free medium for MSCs (NC0103 + NC0105. S, Yocon, Beijing, China) as previously reported,[29] with some modification.

SHED were cultured in a maintenance medium comprising alpha Modification of Eagle's Medium (Gibco, USA) supplemented 10% fetal bovine serum (AusGeneX), 100 U/mL penicillin (Gibco) and 100 U/mL streptomycin (Gibco, USA) at 37 °C in a humidified atmosphere with 5% CO_2. The culture medium was replaced every 3 days. Upon reaching 90% confluence, the cells were digested with 0.05% trypsin-EDTA (Gibco, USA) and passaged. Cells at passages 4−8 were used in the subsequent experiments.[30]

AML12 and RAW264.7 cells were obtained from the cell bank of the Chinese Academy of Sciences. AML12 cells were cultured in a DMEM/F12 medium (Gibco, USA) supplemented with 40 ng/mL dexamethasone (Sigma, USA), 1 × ITS (Gibco, USA), and 10% FBS (Gibco, USA) and were maintained in a CO_2 incubator at 37 °C. When the cell density reached about 80%, cells were detached using 0.25% EDTA-containing trypsin (Solarbio, China) for 2 min, followed by centrifugation at 800 r/min for 5 min, and then subsequent passage.[31] RAW264.7 cells were cultured in a DMEM medium (Gibco, USA) supplemented with 10% FBS (Gibco, USA) and double antibody at 37 °C with 5% CO_2. Upon reaching approximately 80% confluency, the medium was refreshed, and gentle pipet gun agitation was applied to detach the cells from the culture vessel before subculturing.

SHED Osteogenic and Lipogenic Differentiation Assay. SHED were seeded into six-well plates (Corning, USA) and cultured in a growth medium until the cells reached confluence. To induce osteogenic differentiation, the SHED were cultured under osteogenic culture conditions, containing 2 mmol/L β-glycerophosphate, 100 mmol/L L-ascorbic acid phosphate, and 10 nmol/L dexamethasone in a culture medium. Two weeks post induction, 1% Alizarin Red S staining was performed to detect matrix mineralization, followed by observing under a microscope. For adipogenic induction, 500 nmol/L isobutyl methylxanthine, 60 mmol/L indomethacin, 500 nmol/L hydrocortisone, 10 mg/mL insulin, and 100 nmol/L L-ascorbic acid phosphate were added to the growth medium. After 3−4 weeks, the induced cells were stained with Oil Red O and observed under a microscope.[32]

Preparation of SHED-Exo. After reaching 80% fusion, SHED were rinsed twice with PBS and incubated in a serum-free medium (Gibco, USA) for 48 h. The medium was collected, and the supernatant was obtained by centrifuging it at 4 °C for 10 min at 300 g rpm. The obtained supernatant was then centrifuged at 4 °C for 10 min at 2000*g* rpm, and the resulting supernatant was again centrifuged at 4 °C for 30 min at 10,000*g*. Finally, the supernatant was filtered using 0.22um Rapid-Flow Disposable Filter units (Nalgene, USA). Ultrafiltration was performed using Amicon Ultra Centrifugal filters at 4000*g* and 4 °C. To further purify the exosomes, the filtrate was processed using a 30% sucrose/D20 pad in Sterile Quick-Seal Polypropylene tubes (Beckman, USA). The tubes were then centrifuged at 120,000*g* for 70 min at 4 °C. Purified exosomes were extracted, washed several times with PBSs, and then centrifuged at 4000*g* at 4 °C.[33] The resulting exosomes were resuspended in PBS and stored at −80 °C. The exosome size distribution and concentration were determined using nanovision tracking analysis (NTA). Morphological identification of exosomes was done by TEM. Additionally, surface marker proteins of exosome, including CD9, CD81, and TSG101, were analyzed by Western blotting.[20]

Cell Proliferation Assessment. AML12 cells were seeded in 96-well plates at 3000 cells per well and incubated with different concentrations (0, 2, 5, 10 μg/mL) of exosomes for 1, 2, and 3 days. A Cell Counting Kit-8 (CCK-8) (YEASEN, China) solution configured with a cell culture medium at a ratio of 1:10 was added to the cells and incubated for 1 h away from light. Then, the OD values were measured using an enzyme marker. The cell viability was calculated according to the following formula: cell viability = [(experimental wells − blank wells)/(control wells − blank wells)] × 100%.

Scratch Wound Assay. AML12 cells were seeded in 96-well plates and incubated with a medium containing different concentrations of exosomes (0, 5, and 10 μg/mL). When AML12 cells reached approximately 80% confluency, using a sterile pipet tip, a straight scratch was created across the cell monolayer, ensuring uniformity in width and length. At predetermined time points (0, 6, 12, 24, 48, 72, and 96 h), phase-contrast microscopy was used to capture images of the scratched area, ensuring consistent magnification and focus settings throughout the experiment. The area of cells migrating into the scratched area was calculated by using ImageJ software. The formula used to calculate the cell migration rate was as follows: cell migration rate = (initial scratch area − observed scratch area)/initial scratch area. Each set of experiments was repeated three times.

Construction of the ALI Mouse Model. CCl4 was obtained from Macklin Chemical (Shanghai, China). A preconfigured solution of CCl4 was prepared by mixing it with olive oil at a concentration of 1:3 (v/v) and filtered through a 0.22 μm organic filter membrane. Eight-week-old male C57BL/6 mice were weighed individually, and the diluted CCl4 solution was administered at 4 μL/g by intraperitoneal injection. Animals were examined for abnormalities 1 h after injection and once every 24 h thereafter. They were euthanized at 48 h to collect the tissue samples.

Twenty 8-week-old C57/B6 mice were randomly divided into the following four groups: a healthy group without any treatment (control), a group injected intraperitoneally with CCl4 only (CCl4), a control group treated with intraperitoneally injected CCl4 and injected with PBS via the tail vein (CCl4+PBS), and a treatment group injected with CCl4 intraperitoneally and injected with SHED-Exo via the tail vein (CCl4+SHED-Exo). The experimental group was given 0.5 mg/mL SHED-Exo at 0.1 mL each, and the control group was injected with an equal amount of PBS in the tail vein as in the experimental group. After 48 h, all mice were euthanized to collect the liver tissue and blood samples.

RNA Extraction. Total RNA was extracted from the cells utilizing TRIzol Reagent (15596-018; Invitrogen, Carlsbad, CA) and lysed on ice. 20 μL of DEPC water was added to dissolve the RNA, and the Nano Drop 2000 spectrophotometer was employed to assess the concentration of RNA. Subsequently, the total RNA was transcribed into complementary DNA (cDNA) utilizing the Hifair II First Strand cDNA Synthesis kit (Yeasen, China), in accordance with the manufacturer's protocols. Quantification of cDNA was conducted utilizing SYBR Green Master Mix (Yeasen, China) on a Light Cycler 480 instrument.

Western Blot Analysis. Cell and liver tissue samples were lysed using RIPA buffer (Thermo Fisher, USA) supplemented with phosphatase inhibitor (FUDE bio, China) and protease inhibitor (FUDE bio, China) to facilitate protein extraction. The protein concentration was determined using a BCA assay kit (Thermo Scientific, USA). Following adjustment of the protein to a uniform concentration, the samples were denatured by boiling at 100 °C for 10 min with an SDS-PAGE Sample Loading Buffer (FUDE bio, China) and subsequently stored at −20 °C. Protein samples were separated on 4−20% SDS/PAGE gel (ACE, Nanjing). Subsequently, the proteins were transferred onto PVDF membranes (Sigma, USA), which were closed with a rapid closure solution (Beyotime Biotechnology, China) for 30 min. Then, the proteins were incubated with specific primary antibodies at suitable dilutions (1:2000 for internal control antibodies and 1:1000 for others). The protein signal was detected by chemiluminescence. Gray-scale values of the bands were analyzed by using ImageJ software.

Hematoxylin and Eosin and Immunohistochemical Staining. Hematoxylin and eosin (H&E) as well as immunohistochemical (IHC) staining procedures were performed on paraffin-embedded liver sections. Liver tissue was fixed in 4% paraformaldehyde (Sigma, USA) overnight, followed by dehydration, clearing, and embedding in paraffin wax. The paraffin blocks were subsequently sectioned serially at a thickness of 3−5 μm. Following standard deparaffinization, liver

https://doi.org/10.1021/acsami.4c19748
ACS Appl. Mater. Interfaces 2025, 17, 17948−17964

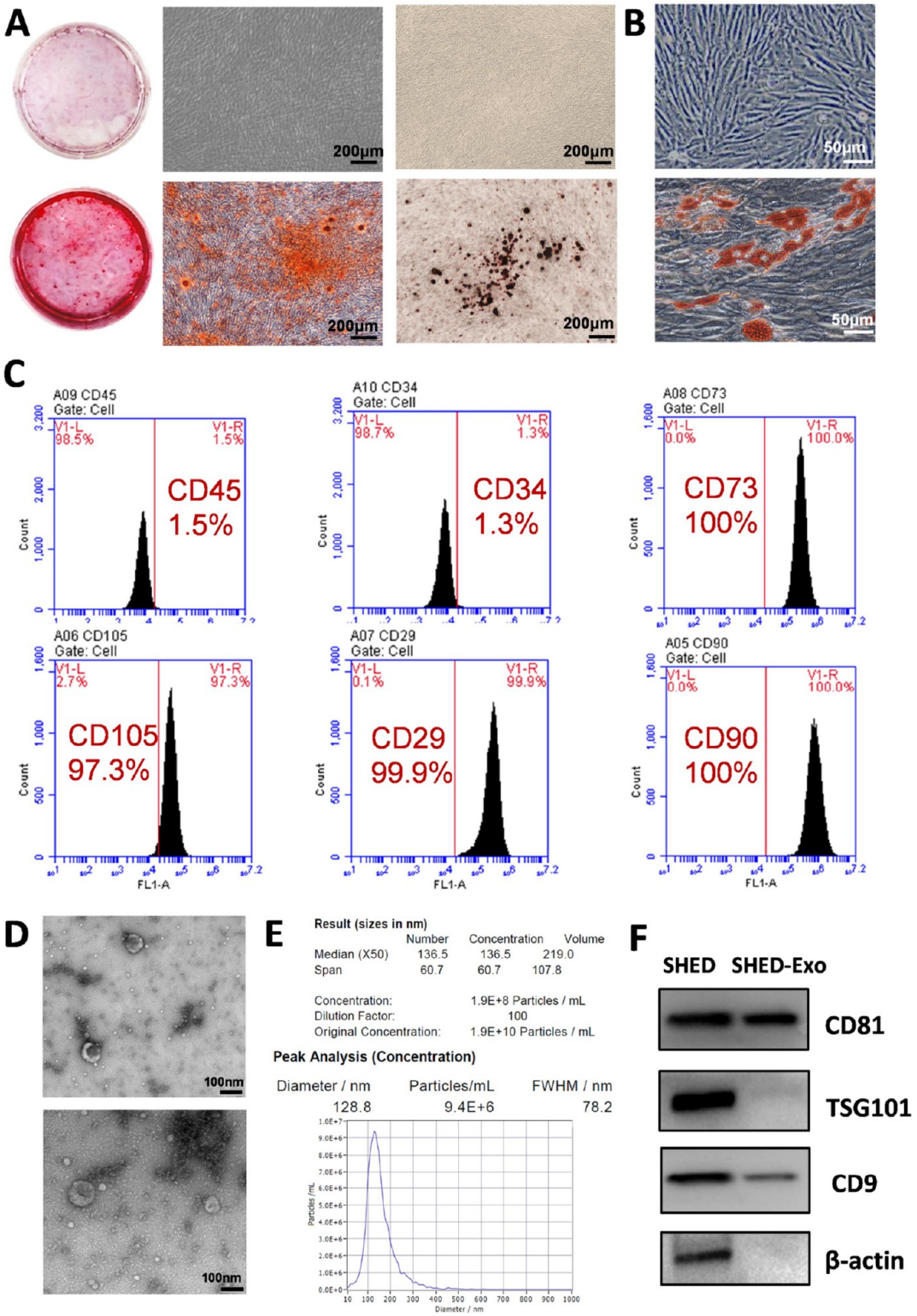

Figure 1. Characterization of SHED and SHED-Exo. (A) Differentiation potential of osteogenesis of SHED was confirmed by Alizarin red staining. (B) Differentiation potential of adipogenesis of SHED was confirmed by Oil Red O staining. (C) SHED-Exo markers CD73, CD105, CD29, and CD90 as well as CD45 and CD34 were detected by flow cytometry. (D) Typical saucer-like morphology of SHED-Exo was captured by transmission electron microscopy. (E) Particle size of SHED-Exo was analyzed by NTA. (F) SHED-Exo was positive for the Exo surface markers CD9 and CD81 by Western Blot (scale bars: 200, 50, and 100 nm).

samples underwent staining with H&E (Sigma, USA) to visualize the histological pattern within necrotic liver areas.

Immunofluorescence Staining. After fixation with 4% paraformaldehyde (Sigma, USA), cell or liver samples were permeabilized with 0.1% Triton X-100 and blocked with 10% bovine serum albumin (BSA). Subsequently, cells were incubated overnight at 4 °C with antibodies diluted in 10% BSA, followed by incubation with the corresponding fluorescent secondary antibodies. Following staining

https://doi.org/10.1021/acsami.4c19748
ACS Appl. Mater. Interfaces 2025, 17, 17948−17964

A

GROUP	DIFF	UP	DOWN
ADSC-Exo vs SHED1-Exo	55	24	31
ADSC-Exo vs SHED2-Exo	42	22	20
ADSC-Exo vs SHED3-Exo	57	28	29
UC-MSC-Exo vs SHED1-Exo	81	45	36
UC-MSC-Exo vs SHED2-Exo	75	38	37
UC-MSC-Exo vs SHED3-Exo	81	44	37
SHED1-Exo vs SHED2-Exo	11	7	4
SHED1-Exo vs SHED3-Exo	18	13	5
SHED2-Exo vs SHED3-Exo	18	6	12

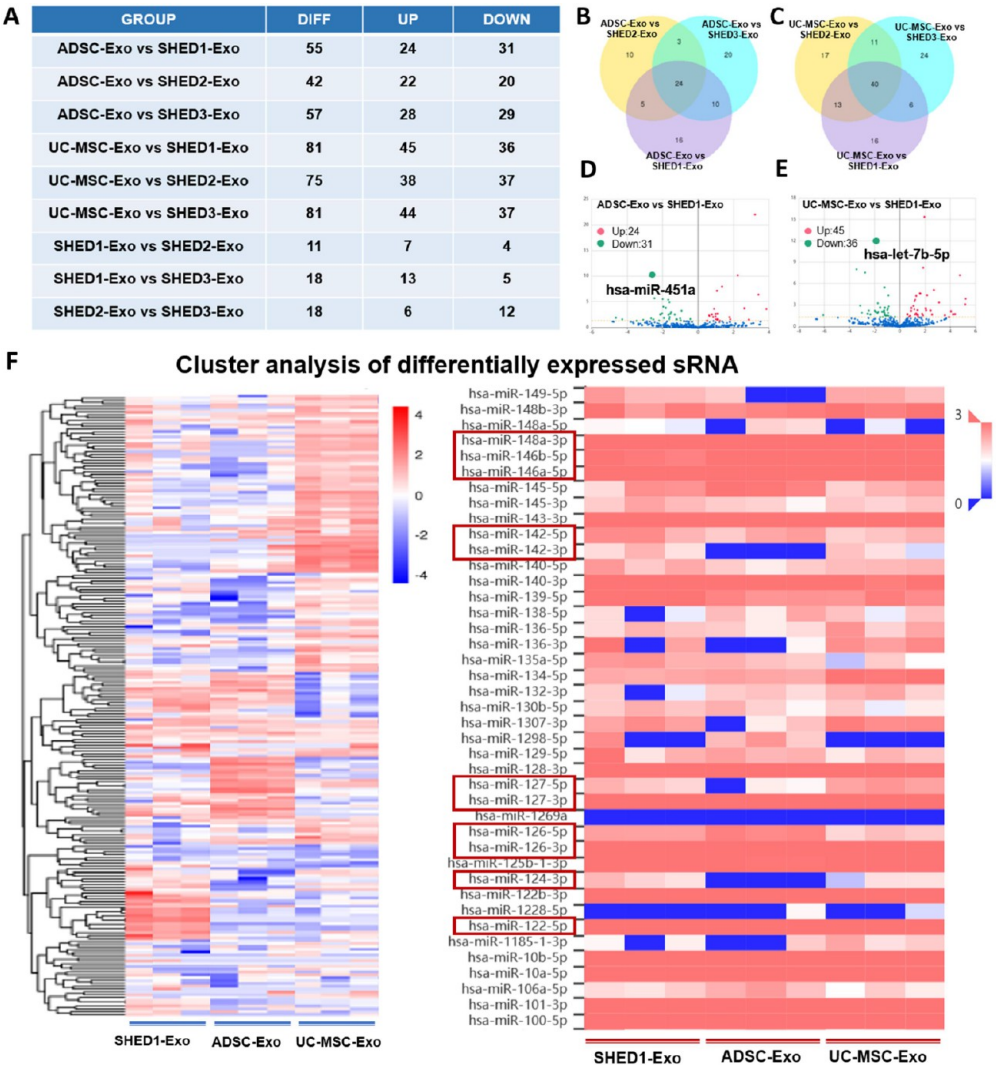

Figure 2. sRNA sequencing analysis of exosomal samples. (A–E) Differential miRNA Venn diagram of sRNA sequencing results of exosomes from ADSC, UC-MSC, and SHED. (F) Cluster analysis of differentially expressed sRNA.

with DAPI (Beyotime Biotechnology, China), cells or liver samples were visualized by using laser scanning confocal microscopy (Leica, USA).

TUNEL Staining. Liver biopsy sections and a well plate were stained using the Situ Apoptosis Detection Kit (Beyotime Biotechnology, China) following the instructions. An antifluorescence quenching sealing solution was employed to observe the plate under a fluorescence microscope immediately after sealing. Cy3 (red fluorescence) exhibited an excitation wavelength of 550 nm and an emission wavelength of 570 nm.

ELISA Assay. The serum samples obtained from the experimental mice were appropriately diluted and combined with a series of known standard concentrations. Subsequently, these mixtures were added to microplate wells precoated with the antigen of interest. The presence and quantity of the target IL-1B and CXCL1 were then determined with ELISA kits (ABclonal, China). Finally, the signal generated was measured using an ELISA plate reader, and the concentrations of IL-1B and CXCL1 in the serum samples were extrapolated based on the standard curve obtained from the known concentrations of the standard solution.

Preparation of GelMA Solution. To prepare a 5% GelMA solution with 0.5% LAP, appropriate amounts of GelMA and LAP powder were accurately weighed based on the desired volume. The mixture was dissolved in PBS at 37 °C in a water bath and then sterilized by filtering through a 0.22 μm membrane. The solution was stored, protected from light, until further use.

Synthesis of the GelMA@SHED-Exo Hydrogel. For the preparation of the GelMA@SHED-exo hydrogel, the required amounts of GelMA and LAP powder were weighed according to the solution volume. SHED-Exo at a predetermined concentration was added into PBS as a solvent, and the powders were dissolved in a 37 °C water bath. Sterilization was performed by filtering, and then the solution was exposed to UV light at 365 nm with an intensity of 2 W/cm^2 for approximately 10 s to cross-link and form the GelMA@SHED-exo hydrogel.

Cell Culture on Biomaterial Surfaces. GelMA and GelMA@SHED-exo hydrogels were prepared in a 24-well plate as described above. AML12 cells were digested to create a suspension at a concentration of 5 × 10^5 cells/mL. 1 mL of this cell suspension was added to each well and mixed thoroughly before placing the plate in an incubator. Once cells adhered, their morphology was observed under a microscope. The cells were stained with a live/dead assay kit, and cell viability was assessed using fluorescence microscopy.

Live/Dead Staining Procedure. Calcein-AM and PI solutions were prepared using a buffer. The cell culture medium was removed from the wells and replaced with the staining solutions. The cells were incubated at 37 °C for 45 min, washed twice with PBS, and then observed and photographed under a fluorescence microscope.

https://doi.org/10.1021/acsami.4c19748
ACS Appl. Mater. Interfaces 2025, 17, 17948−17964

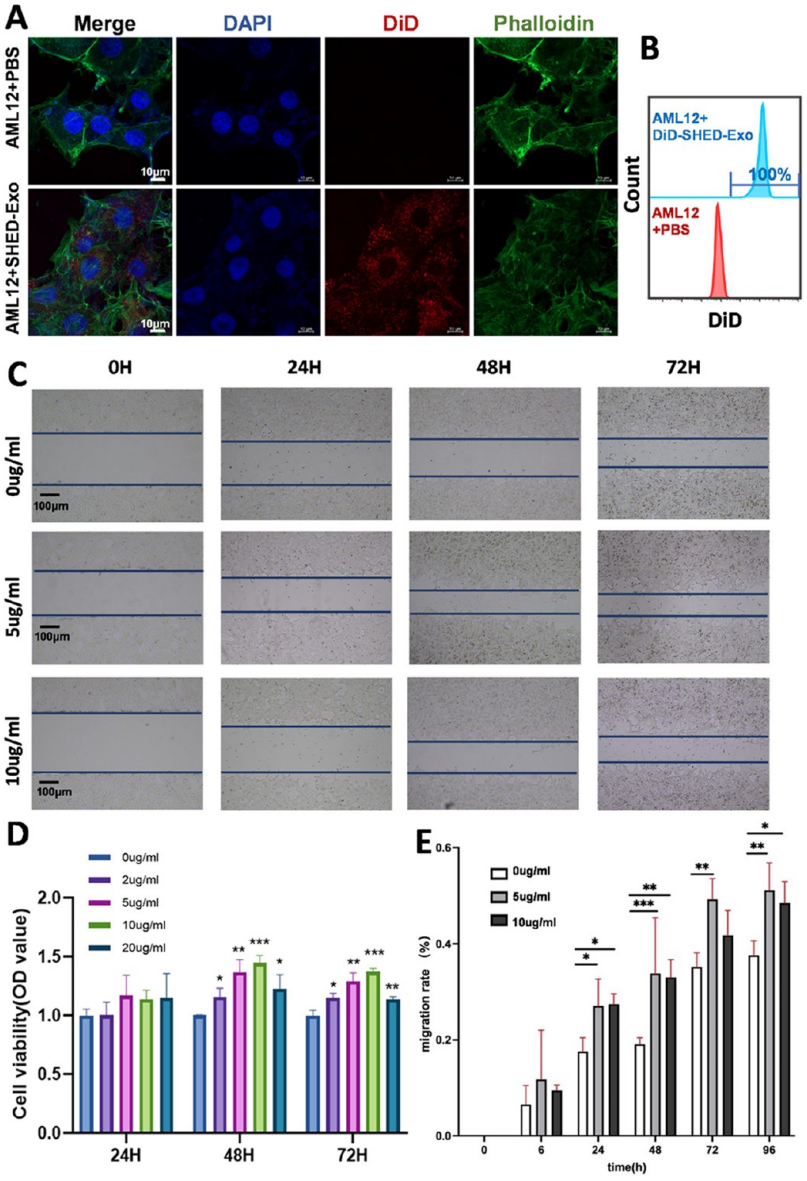

Figure 3. SHED-Exo promotes hepatocyte proliferation and migration in vitro. (A) Fluorescent images of SHED-Exo uptake by AML12 cells. (B) Flow cytometric analysis of the percentage of AML12 cells that have internalized exosomes. (C) Migration rate of AML12 treated with SHED-Exo (0, 5, 10 μg/mL) was tested by the scratch wound assay. (D) Cell proliferation rate of AML12 treated with SHED-Exo (0, 5, 10 μg/mL) was detected by the CCK-8 assay. (E) Quantitative analysis of the wound healing assay (n = 5; *p < 0.05, **p < 0.01, ***p < 0.001, scale bars: 10 μm, 100 μm).

Bile Duct Ligation (BDL) Model Construction. A section of the bile duct was gently isolated using micro forceps, and a 6−0 surgical suture was placed around the middle of the isolated section. After the suture was secured, the bile duct was severed between the two ligation points. GelMA@SHED-exo hydrogel was applied directly onto the liver surface in the treatment group, while the control group received only the GelMA hydrogel.

Statistical Analysis. Statistical analysis was conducted utilizing GraphPad Prism v8.0 software. Each experiment subjected to statistical scrutiny entailed a minimum of three or more independent replications or the formation of three groups of replications. Experimental outcomes were presented as mean ± standard deviation (SD) values. The evaluation of differences among more than two groups was carried out using one-way ANOVA. The "*" symbol denotes p-values: *p < 0.05; **p < 0.01; and ***p < 0.001. A significance level of p < 0.05 was considered statistically significant. Bioinformatic analysis was performed using the OmicStudio tools and Novomagic tools.

RESULTS AND DISCUSSION

Characterization of SHED and SHED-Exo. SHED exhibit remarkable pluripotency and self-renewal capabilities. Additionally, SHED represent a plentiful and readily obtainable source of MSCs in comparison to other alternative sources.[23] Morphologically, SHED exhibited a spindle-shaped, fibroblast-like appearance under light microscopy, consistent with the characteristic morphology of MSCs. Further assessment of the differentiation capacity revealed that following 21 days of osteogenic-lipogenic induction, SHED effectively differentiated into osteoblasts and adipocytes, as evidenced by the conspicuous formation of red mineralized nodules and characteristic orange-red Oil Red O staining, respectively, thus confirming the multipotency of SHED (Figure 1A,B). Flow cytometry analysis of SHED revealed the robust expression of positive markers, including CD29 (99.9%), CD73 (100%),

https://doi.org/10.1021/acsami.4c19748
ACS Appl. Mater. Interfaces 2025, 17, 17948−17964

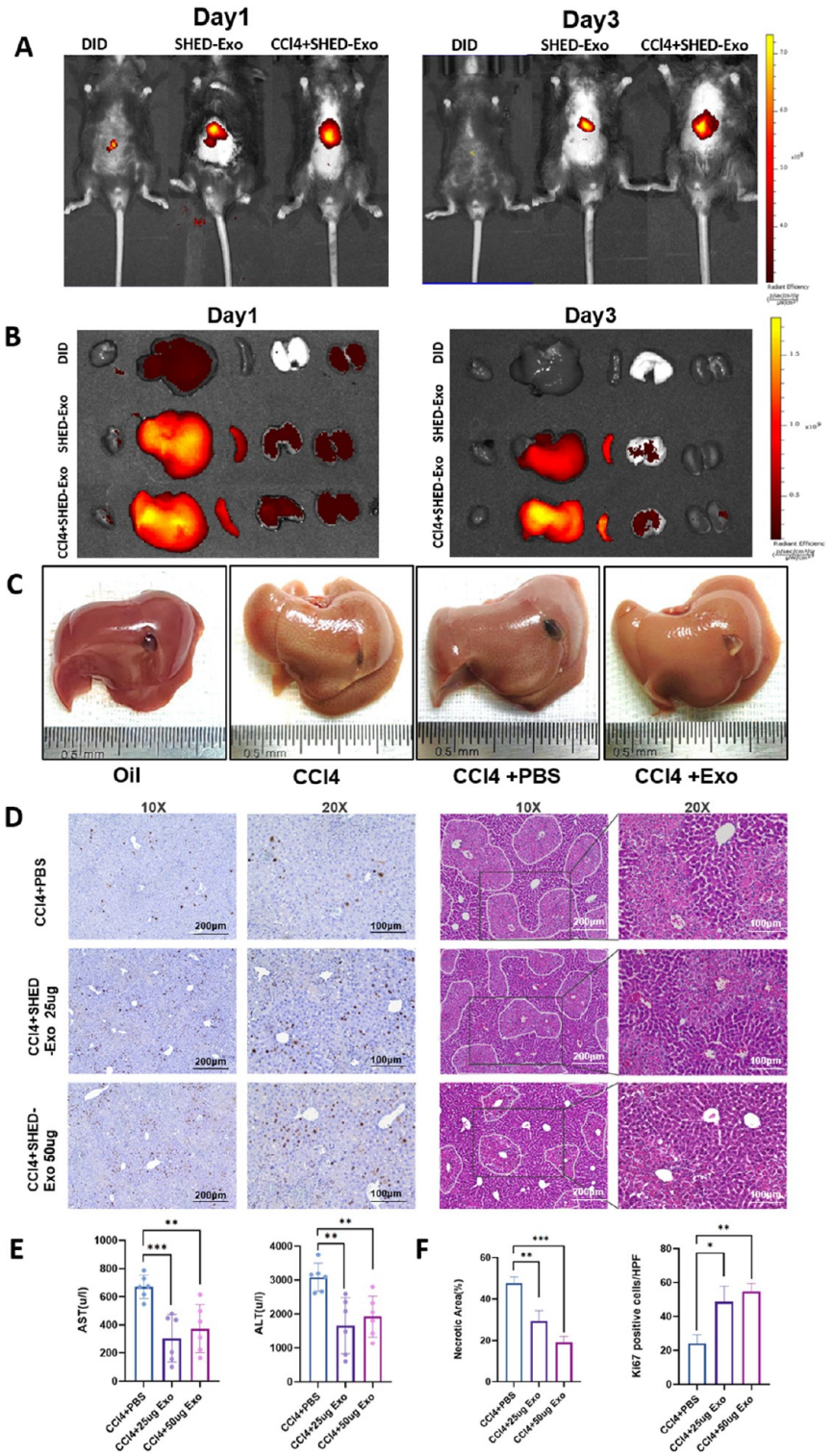

Figure 4. SHED-Exo promotes hepatocyte proliferation and migration in vivo. (A) Fluorescence intensity imaging of DiD or DiD-labeled SHED-Exo groups at 24 and 72 h. (B) Fluorescence quantification of isolated organs from the SHED-Exo group at 24 and 72 h. (C) Gross appearance of the liver tissues from oil, CCl_4, CCl_4+PBS, and SHED-Exo-treated groups. (D) Ki67 and H&E staining of liver tissues from CCl_4, and CCl_4 mice with SHED infusion groups and the quantitative analysis. (E) Levels of serum ALT and AST of CCl_4 and SHED-Exo-treated groups. (F) Quantitative analysis of the necrotic area and Ki67-positive cell count of mouse liver sections (n = 5; *p < 0.05, **p < 0.01, ***p < 0.001, scale bars: 200 μm, 100 μm).

CD90 (100%), and CD105 (97.3%), while negative markers such as CD45 (1.5%) and CD34 (1.3%) were minimally expressed (Figure 1C). High-quality exosomes were isolated from the SHED medium by utilizing gradient ultracentrifugation. Subsequent observation of the SHED-exosomal morphology was conducted via transmission electron microscopy, and protein analysis was performed for further characterization. The examination revealed a characteristic saucer-like shape of

https://doi.org/10.1021/acsami.4c19748
ACS Appl. Mater. Interfaces 2025, 17, 17948−17964

the isolated exosomes, characterized by a peak particle size of 128.8 nm and an average particle size of 136.5 nm (Figure 1D,E). Western blot analysis demonstrated that SHED-Exo exhibited positivity for canonical exosomal markers, including CD9 and CD81, whereas SHED-Exo exhibited a faint positivity with indistinct bands that could be attributed to the pronounced expression of TSG101 within the originating cells (Figure 1F). In summary, these findings collectively affirm the successful isolation of SHED-Exo.

sRNA Sequencing Analysis of Exosomal Samples. Extensive research has been conducted to determine the factors influencing MSC efficacy, including cell source, donor age, and gender, to achieve optimal therapeutic outcomes.[34] Donor age is particularly significant as MSC potency diminishes with age, with cells from older donors displaying increased senescence and reduced differentiation potential.[35] The characteristics of SHED necessitate that the donors are exclusively young individuals. Moreover, MSCs derived from different tissue sources exhibit variations in differentiation potential, proliferation rates, immunomodulatory properties, and gene expression profiles.[36] In our study, we extracted exosomes from BMSCs, UC-MSC, and SHED for sRNA sequencing.[37] The analysis revealed that exosomes derived from the same MSC source exhibited reduced interindividual variability compared to those obtained from different tissue sources, with each tissue type demonstrating unique miRNA enrichment patterns (Figure 2A−E). Previous research has shown that exosome miRNA levels increase proportionally with cell proliferation, facilitating noninvasive and straightforward assessment of cell differentiation through miRNA ratio detection.[38] Given the challenges posed by batch-to-batch variability in exosomes for clinical translation, miRNA profiling offers a promising solution for quality control.

Selecting some differential miRNA clustering, we found that all three cell-derived exosomes expressed miRNAs with therapeutic potential in tissue repair, such as miR-148a-3p, which improves hepatocyte proliferation and liver regeneration, and miR-122-5p,[39,40] which promotes angiogenesis. In addition, we also noted that a large number of highly and differentially expressed miRNAs were associated with the regulation of macrophage polarization, such as miR-126-3p,[40] miR-124-3p,[41,42] miR-142-5p,[43] and the miR-146 family members, miR-146a-5p and miR-146b-5p. These inhibitory miRNAs can modulate the activity of downstream pathways such as the NF-κB pathway, thereby reducing proinflammatory cytokines or reversing the polarization state of macrophages (Figure 2F). The potential of all three cellular sources of exosomes to modulate macrophage influence on the inflammatory response gives us some direction for the study of exosomes of SHED.[37]

SHED-Exo Promotes Hepatocyte Proliferation and Migration In Vitro. DiD prelabeled exosomes were coincubated with AML12 cells for 24 h. Both fluorescent images and flow cytometric results suggest that all hepatocytes are capable of internalizing exosomes (Figure 3A,B). Subsequently, we assessed the effect of SHED-Exo on AML12 proliferation through CCK-8 experiments. The exosome coincubation groups (5 and 10 μg/mL) exhibited a significant enhancement in AML12 proliferation, with statistically significant differences ($p < 0.05$) (Figure 3D). After incubating AML12 with different concentrations of SHED-Exo (0, 5, and 10 μg/mL), a scratch wound assay revealed that both 5 μg/mL ($p < 0.01$) and 10 μg/mL ($p < 0.05$) SHED-Exo promoted AML12 migration compared to the control wells (Figure 3C,E). Moreover, the migratory capacity of AML12 cells did not exhibit a concentration-dependent increase with escalating exosome concentrations (from 5 to 10 μg/mL). These findings collectively indicate that SHED-Exo effectively stimulates AML12 migration and proliferation, prompting further investigation into the impact of SHED-Exo on ALI.

SHED-Exo Treatment Attenuates Acute Liver Injury In Vivo. Motivated by the in vitro efficacy of SHED-Exo, we proceeded to explore the impact of SHED-Exo on CCl4-induced ALI in vivo. To visualize the biodistribution of DiD-labeled exosome to assess whether SHED-Exo preferentially accumulates in the damaged liver, we used the IVIS imaging system to monitor the distribution of DiD-labeled SHED-Exo in both damaged and healthy livers at 24 and 72 h after tail vein injection.[44] Noninvasive real-time live imaging of the SHED-Exo-treated mice revealed that the liver fluorescence signals were stronger in ALI mice compared to the PBS or oil groups (Figure 4A), suggesting a propensity for circulating SHED-Exo to accumulate within damaged hepatic tissues and exhibit prolonged retention. Furthermore, ex vivo imaging of excised major organs corroborated the presence of fluorescence signals, specifically within the liver (Figure 4B). Robust fluorescence persisted up to 72 h, effectively illustrating the targeting specificity and prolonged circulation properties of SHED-Exo. While modification of the membrane structure may be required to enhance organ-specific targeting when utilizing SHED-Exo for treatments of nonhepatic ailments, this inherent liver tropism represents a beneficial attribute for managing liver diseases, affording precise targeting and efficacious support within the period of ALI.

Observation of hepatic morphology post CCl4 injection revealed a paler hue compared to healthy livers, with evident granular formations on the liver surface in CCl4 and CCl4+PBS groups compared to the SHED-Exo-treated group (Figure 4C). Initial observation of liver injury by HE staining demonstrated extensive peri-central venous hepatocellular necrosis alongside pronounced immune cell infiltration in the CCl4+PBS group (Figure 4D,F). Notably, the CCl4+SHED-Exo group displayed a significant reduction in necrotic areas surrounding the central vein, approaching the architecture of normal liver tissue. Concurrently, alanine aminotransferase (ALT) and aspartate aminotransferase (AST) levels mirrored the histological findings (Figure 4E). Concomitantly, IHC analysis of Ki67 expression in liver tissue sections at 48 h post-treatment was conducted. The number of Ki67-positive cells was notably increased in the CCl4+SHED-Exo group compared to the CCl4+PBS group (Figure 4D,F). The above results indicate a potential influence of SHED-Exo on the process of liver regeneration following ALI.

RNA Sequencing Analysis of Liver Sample. Through the above preliminary assessment of injury area, liver function, and liver regeneration, it was concluded that SHED-Exo had some therapeutic effect on ALI, and further exploration of the mechanism was considered. A sufficient amount of liver tissue was taken to extract RNA for whole transcriptome sequencing,[45] of which there were three in each group of CCl4+PBS and CCl4+SHED-Exo. 524 differentially expressed genes (DEGs) were found in liver genes in the treatment group out of a total of 22,798 genes sequenced for CCl4+SHED-Exo compared with CCl4+PBS, and 260 genes were upregulated and 264 genes were downregulated (Figure 5A). Then, the biological significance of the relevant DEGs was

https://doi.org/10.1021/acsami.4c19748
ACS Appl. Mater. Interfaces 2025, 17, 17948−17964

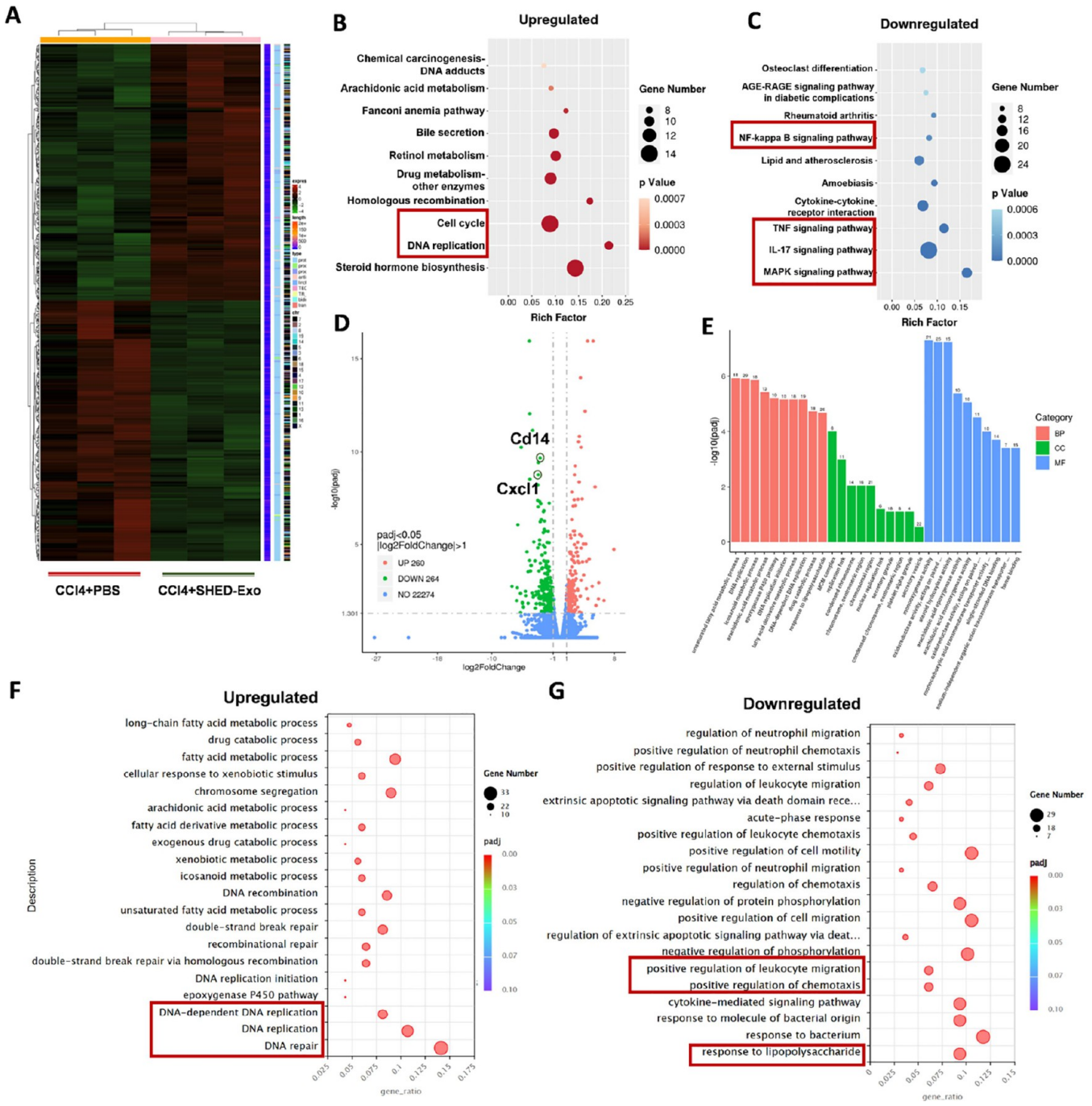

Figure 5. RNA sequencing analysis of liver sample. (A) Clustering heat map of DEGs. (B, C) Scatter plot representation of the KEGG pathway enrichment analysis. (D) Volcano plot analysis of differential gene expression. (E) Histogram visualization of gene ontology enrichment analysis. (F, G) Scatter plot illustrating gene ontology enrichment analysis.

further explored by Gene Ontology enrichment analysis and KEGG pathway enrichment analysis, and it was found that the downregulated genes were mainly in the pathways related to inflammatory cell migration, extrinsic apoptotic signaling pathway, and positive regulation of chemokines, which indicated that the liver showed different degrees of decreases in the recruitment of inflammatory cells, apoptosis, and inflammatory response after SHED-Exo treatment, and to a certain extent, it confirmed the HE staining observation that the immune cell infiltration in the necrotic region of the liver coincided. In addition, the upregulated DEGs were mainly in the cell cycle and DNA replication-related pathways, which was consistent with the Ki67 IHC staining results, and the upregulated DEGs also contained drug metabolism and bile secretion pathways (Figure 5B–G), suggesting that the regenerative ability of liver cells and liver function were indeed affected after SHED-Exo treatment. It is not difficult to see that liver function is severely impaired in ALI, and the liver bears a huge load of simultaneously regenerating liver cells and exercises liver function in the presence of an inflammatory response, in which SHED-Exo treatment may act from multiple angles to realize its therapeutic effects in multiple pathways. One of the most popular perspectives is the regulation of immune cells by SHED-Exo, and the top four

https://doi.org/10.1021/acsami.4c19748
ACS Appl. Mater. Interfaces 2025, 17, 17948−17964

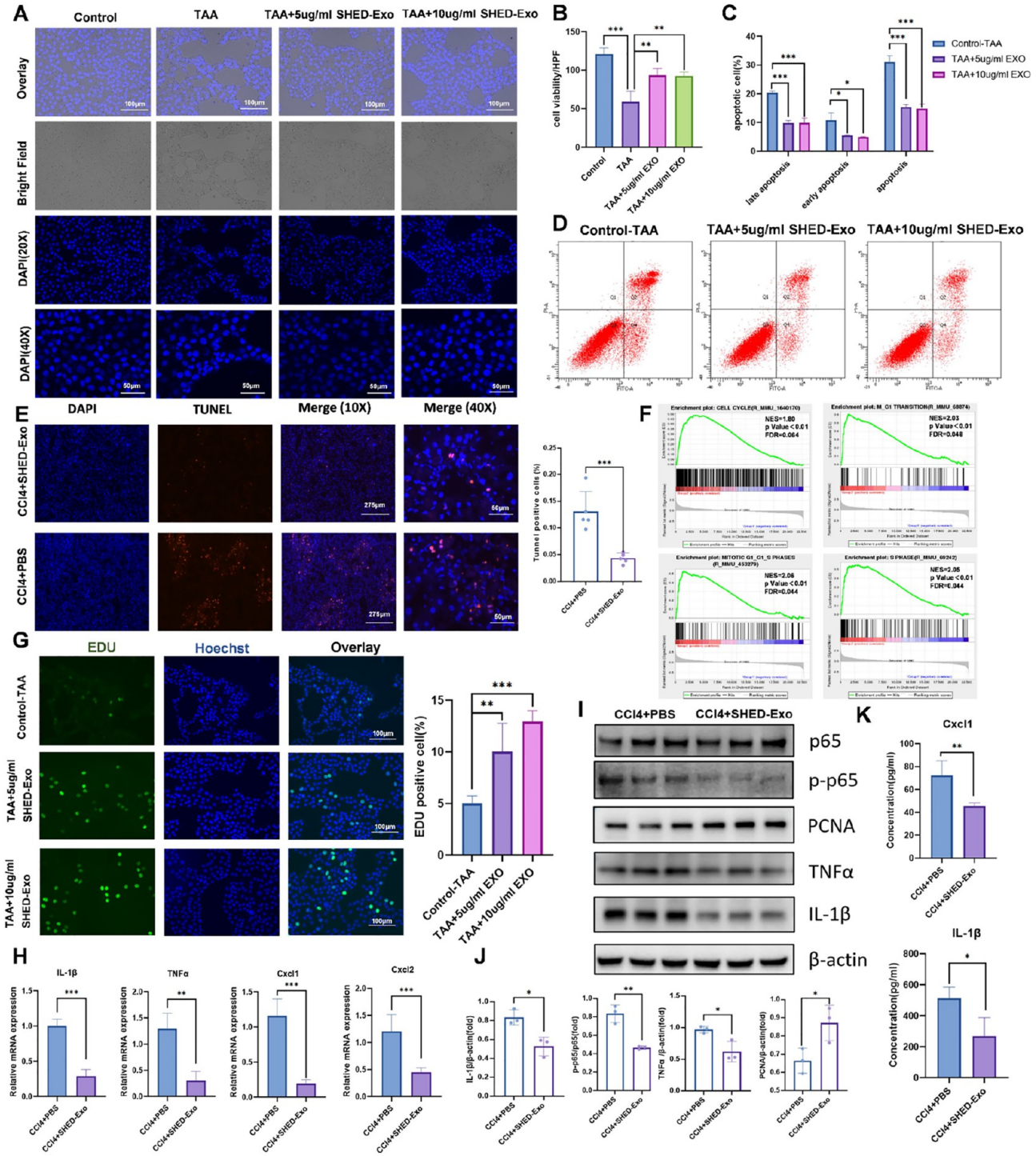

Figure 6. SHED-Exo protects hepatocytes during injury. (A, B) Following TAA-induced damage, the cell count was evaluated after 24 h of culture with SHED-Exo. (C, D) AML12 cell apoptosis of control, TAA+5 μg/mL SHED-Exo, and TAA+10 μg/mL SHED-Exo groups was analyzed by flow cytometric analysis. (E) TUNEL staining of the CCl4+PBS group and the CCl4+SHED-Exo group. (F) Effect of SHED-Exo treatment on transitions in multiple phases of the cell cycle by GSEA analysis. (G) EdU staining to analyze the proliferation-promoting effect of SHED-Exo on hepatocytes. (H) Expression of Cxcl1, Cxcl2, IL-1β, and TNF-α by qRT−PCR in CCl4+PBS and CCl4+SHED-Exo mice. (I, J) Western blotting analysis of the expression of p65, p-p65, PCNA, IL-1β, and TNF-α. (K) ELISA detects concentrations of IL-1β and Cxcl1 in the serum (n = 3; *p < 0.05, **p < 0.01, ***p < 0.001, scale bars: 275, 100, 50 μm).

downregulated pathways enriched in the KEGG analysis results were IL-17, MAPK, TNF, and NF-kappa B pathways, all of which are closely related to immune responses (Figure 5C). Further exploration of these pathway-associated DEGs revealed significant downregulation of IL-1b as well as Cxcl1, Cxcl2, and Cxcl5 in the chemokine family.[46] Chemokines make up a class of cytokine proteins that act as important signaling molecules to regulate immune and inflammatory responses, and the degree of chemokine upregulation is often consistent with the phenotype of worsening liver injury. On

https://doi.org/10.1021/acsami.4c19748
ACS Appl. Mater. Interfaces 2025, 17, 17948−17964

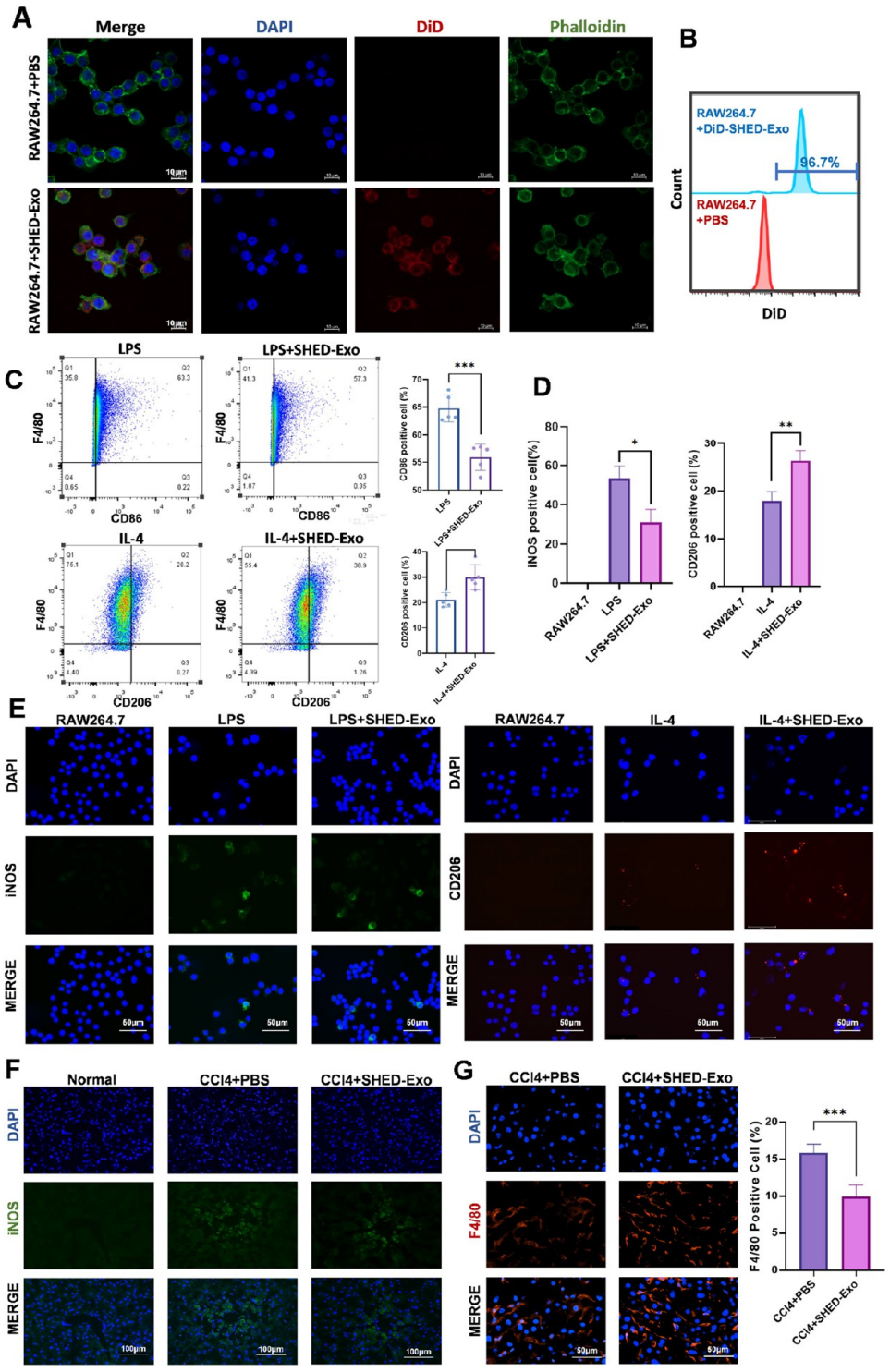

Figure 7. SHED-Exo ameliorates inflammatory response by remodeling the macrophage phenotype. (A) Fluorescent images of SHED-Exo uptake by RAW264.7 cells. (B) Flow cytometric analysis of the percentage of RAW264.7 cells that have internalized exosomes. (C) Flow cytometry analysis of the polarization state of RAW264.7 cells after LPS, IL-4, LPS+SHED-Exo, and IL-4+SHED-Exo induction. (D) Fluorescent staining of RAW264.7 after LPS and IL-4 stimulation with the iNOS antibody and CD206 antibody to identify the polarization ratio of macrophages. (E) Quantification of the iNOS$^+$ and CD206$^+$ RAW264.7. (F) Fluorescent staining of CCl4+PBS, and CCl4+SHED-Exo group mice with the iNOS antibody. (G) Fluorescent staining of normal, CCl4+PBS, and CCl4+SHED-Exo group mice with F4/80 (n = 3; *p < 0.05, **p < 0.01, ***p < 0.001, scale bars: 10, 50, 100 μm).

the differential gene volcano plot, it can be observed that among the top 10 genes downregulated in the treatment group compared with the CCl4+PBS group was Cd14 in addition to Cxcl1 (Figure 5D), suggesting that SHED-Exo treatment may be closely related to the regulation of macrophages.[47] Taken together, the above data suggest that SHED-Exo treatment indeed improves the liver regeneration in vivo by down-regulating inflammatory response and immune cell recruitment

https://doi.org/10.1021/acsami.4c19748
ACS Appl. Mater. Interfaces 2025, 17, 17948−17964

and promotes cell regeneration within the liver, thus realizing its therapeutic effect. The next step is to consider continuing to investigate whether SHED-Exo can directly act on hepatocytes to promote cell proliferation and liver tissue regeneration in response to hepatocyte injury in vivo and in vitro and to clarify whether it can affect macrophage recruitment and phenotypic changes.

SHED-Exo Protects Hepatocytes during Injury, Reduces Their Apoptosis, and Promotes Proliferation both In Vivo and In Vitro. Given the tendency of carbon tetrachloride (CCl4) to precipitate from the culture medium, even when cosolubilized with dimethyl sulfoxide, thioacetamide (TAA) was chosen for in vitro experiments to establish a more consistent and soluble model of hepatocyte injury. Due to the interference caused by TAA reduction in assays such as CCK-8, DAPI staining was initially employed to observe the effect of SHED-Exo on the number of AML12 cells within a single high-magnification field of view in the TAA-induced injury model. After incubating AML12 cells with TAA and different concentrations of SHED-Exo (5 and 10 μg/mL) for 24 h, their nuclei were stained with DAPI, and the number of cells in high-magnification fields was then quantified using fluorescence microscopy. Results showed a reduced cell count in the SHED-Exo group compared to the noninjured group but notably higher than the TAA-injured group (Figure 6A,B). To investigate whether SHED-Exo directly mitigates hepatocyte apoptosis induced by TAA in AML12 cells in vitro, Annexin V−PI apoptosis flow cytometry was employed to assess the apoptosis rate. Results indicated that following intervention with varying concentrations of SHED-Exo the proportions of early and late apoptotic cell populations were lower compared to the control group ($p < 0.05$) (Figure 6C,D). While exosomes exhibit the capability to diminish apoptosis in hepatocytes, the efficacy of SHED-Exo in reducing apoptosis did not demonstrate a notable discrepancy between high and low concentrations. In summary, this suggests that SHED-Exo can directly mitigate hepatocyte apoptosis in acute injury settings. TUNEL fluorescence staining corroborated the pronounced hepatocyte apoptosis triggered by CCl4, while the administration of SHED-Exo notably diminished the number of apoptotic hepatocytes surrounding the central vein (Figure 6E). The TUNEL assay demonstrated the hepatocyte apoptosis-reducing effects of SHED-Exo in vivo.

According to the RNA-seq findings, SHED-Exo not only modulates apoptosis but also facilitates DNA damage repair. Furthermore, GSEA analysis revealed that SHED-Exo treatment during in vivo experiments influences various stages of the cell cycle, encompassing transitions such as the S-phase, G1/S-phase, and M/G1-phase. Subsequent in vitro investigations involving EdU staining analysis aimed to elucidate its impact on hepatocyte proliferation by examining the cell cycle (Figure 6F). EdU, a thymine nucleoside analogue, was utilized to quantify cells undergoing DNA replication, indicative of the S-phase. The EdU staining results demonstrated a notably elevated proportion of EdU-positive cells following treatment with different concentrations of SHED-Exo compared to the control group ($p < 0.05$) (Figure 6G). Interestingly, there was no discernible variance in the efficacy of SHED-Exo across different concentration interventions. These findings confirm the ability of SHED-Exo treatment to expedite cell-cycle progression and foster hepatocyte proliferation to a certain extent.

All conducted experiments collectively indicate the positive impact of SHED-Exo intervention on reducing hepatocyte apoptosis and enhancing hepatocyte proliferation, both in vivo and in vitro. Western blotting analysis showed a significant upregulation of PCNA expression in the treated group, providing additional confirmation that SHED-Exo can influence various stages of the cell cycle (Figure 6I,J). Collectively, these findings suggest that SHED-Exo may expedite liver injury repair following ALI by safeguarding hepatocytes from apoptosis and stimulating hepatocyte cycle activity.

In the prognosis of ALI, the production of inflammatory factors and the infiltration of inflammatory cells play crucial roles. Analysis of liver tissue mRNA levels revealed a significant reduction in TNF-α, IL-1β, Cxcl1, and Cxcl2 in the SHED-Exo treatment group compared to the CCl4 group (Figure 6H). ELISA assays further demonstrated that CCl4 treatment notably increased serum levels of inflammatory factors and chemokines, including IL-1β and Cxcl1 (Figure 6K). Conversely, SHED-Exo mitigated the elevation of these inflammatory cytokines in both serum and liver tissues in CCl4-induced ALI. This suggests that SHED-Exo may suppress systemic and hepatic inflammation in CCl4-induced ALI mice. Western blotting revealed a significant reduction in IL-1β expression in the treated tissues (Figure 6I,J).

SHED-Exo Ameliorates Inflammatory Response by Remodeling Macrophage Phenotype. Macrophages play a pivotal role in the initiation, perpetuation, and resolution of tissue damage, with macrophage polarization closely linked to the progression of liver disease.[48,49] Based on the observations presented above, we investigated the regulatory effects of SHED-Exo on macrophages. Additionally, we aimed to determine whether macrophages can internalize SHED-Exo. In vitro, we utilized mouse-derived macrophages RAW264.7 and incubated them with DiD prelabeled exosomes for 24 h. Confocal microscopy images demonstrate that SHED-Exo can be internalized by RAW264.7 cells (Figure 7A). Flow cytometry results further indicate that nearly all RAW264.7 cells possess the capability of internalizing SHED-Exo (Figure 7B).

To assess the impact of SHED-Exo on macrophages, we employed lipopolysaccharide (LPS) to induce M1 polarization and interleukin-4 (IL-4) to induce M2 polarization in RAW264.7 cells.[41,50] Subsequently, we examined the expression of M1 (CD86) and M2 (CD206) macrophage polarization markers in the presence or absence of SHED-Exo (10 μg/mL). Flow cytometry analysis revealed a statistically significant reduction in the population of F4/80$^+$CD86$^+$ cells in the SHED-Exo group compared to the control group, while F4/80$^+$CD206$^+$ cells were significantly elevated in the SHED-Exo group (Figure 7C). Additionally, the macrophage polarization ratio was determined by using cellular immunofluorescence, wherein RAW264.7 cells stimulated with LPS and IL-4 were stained with the iNOS antibody (M1) and CD206, respectively. Immunofluorescence staining indicated a marked decrease in M1 macrophages following SHED-Exo treatment compared to the control group,[51] along with an increase in M2 macrophages (Figure 7D,E). In summary, SHED-Exo demonstrated the ability to attenuate macrophage polarization toward the M1 phenotype while promoting polarization toward the M2 phenotype. Furthermore, immunofluorescence staining targeting iNOS (M1 marker) indicated enhanced infiltration of iNOS-positive cells in the CCl4+PBS

https://doi.org/10.1021/acsami.4c19748
ACS Appl. Mater. Interfaces 2025, 17, 17948−17964

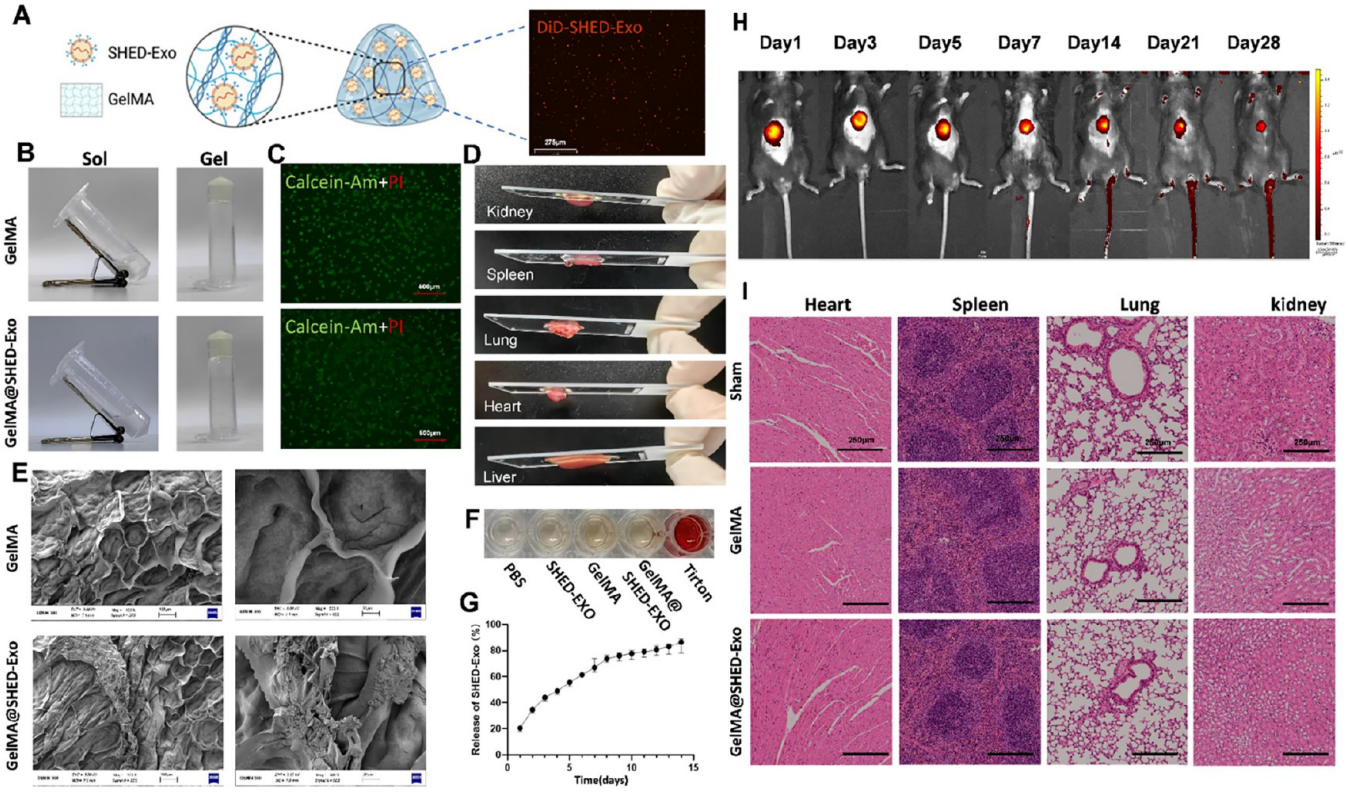

Figure 8. Characterization of GelMA@SHED-Exo. (A) Schematic and fluorescence microscopy images of GelMA@SHED-Exo (the figure was generated with BioRender). (B) GelMA@SHED-Exo gelation performance. (C) Live/dead cell staining. (D, E) Microscopic morphology and adhesion properties. (F) Hemolysis test results. (G) Release curve of GelMA@SHED-Exo. (H) In vivo degradation imaged by live imaging. (I) In vivo safety assessment of GelMA@SHED-Exo (scale bars: 500, 275, 250, 100, 20 μm).

group, with fewer observed in the SHED-Exo group (Figure 7F). Collectively, these data suggest that SHED-Exo administration facilitates macrophage remodeling and exerts an anti-inflammatory effect in the liver of ALI mice, thereby transforming the proinflammatory M1 microenvironment of ALI into an M2 anti-inflammatory milieu conducive to tissue regeneration. Based on these findings, further exploration of the mechanisms underlying inflammation inhibition was conducted with a focus on the NF-κB signaling pathway, a key regulator of inflammation during liver injury. Interestingly, the liver tissue of mice in the CCl4 group showed a substantial accumulation of F4/80 macrophages, whereas macrophage infiltration in the SHED-Exo administration group was significantly reduced (Figure 7G).

Characterization of GelMA@SHED-Exo. The GelMA@SHED-Exo hydrogel is solidified through rapid UV-induced cross-linking in the presence of the photoinitiator LAP. Fluorescence microscopy revealed the uniform distribution of DiD-labeled SHED-Exo within GelMA (Figure 8A). Both GelMA and GelMA@SHED-Exo exist as liquid solutions before UV exposure, forming hydrogels within 10 s under UV light (Figure 8B), indicating that the encapsulation of SHED-Exo does not impair the gelation process. After seeding digested AML12 cells onto hydrogels, cells adhered to the surface within 1 day. Live/dead staining on day 2 confirmed high cell viability, with no PI-positive dead cells observed in either group (Figure 8C). Adhesion tests on ex vivo organs demonstrate that GelMA@SHED-Exo exhibits strong adhesion, enabling effective SHED-Exo delivery (Figure 8D). Scanning electron microscopy reveals that GelMA has a uniformly distributed, porous structure with an average pore size of 100 ± 20 μm (Figure 8E). We derived conclusions consistent with prior research,[52] indicating that the microstructure of GelMA@SHED-Exo remains largely unchanged. This suggests that SHED-Exo exerts no significant influence on the porosity of GelMA. Hemolysis assays indicate that GelMA@SHED-Exo does not induce hemolysis (Figure 8F). Ex vivo analysis indicated a stable release of SHED-Exo over 2 weeks (Figure 8G). Even 28 days post subcutaneous implantation, SHED-Exo within GelMA@SHED-Exo retained detectable fluorescence, demonstrating prolonged retention and sustained release (Figure 8H). Histological analysis post implantation showed no significant pathological changes in major organs, confirming the in vivo safety of GelMA@SHED-Exo (Figure 8I).

Controlled Release of SHED-Exo for Liver Fibrosis Treatment. To evaluate the therapeutic effects of GelMA@SHED-Exo on liver fibrosis, a BDL mouse model was established with four groups: Sham, BDL, BDL+GelMA, and BDL+GelMA@SHED-Exo (Figures 9A,B,D). Over 2 weeks, survival rates were recorded, and samples were collected on day 14. Mice treated with GelMA@SHED-Exo exhibited significantly improved survival (Figures 9C). Histological analysis using HE staining revealed that in the Sham group, liver lobules had clear structures with no fibrosis, while in the BDL group, marked peribiliary fibrosis and nodular changes were observed, progressing toward bridging fibrosis. The GelMA group showed no significant improvement, mirroring that of the BDL group. However, in the GelMA@SHED-Exo group, fibrosis was notably reduced, with only minimal nodular

https://doi.org/10.1021/acsami.4c19748
ACS Appl. Mater. Interfaces 2025, 17, 17948−17964

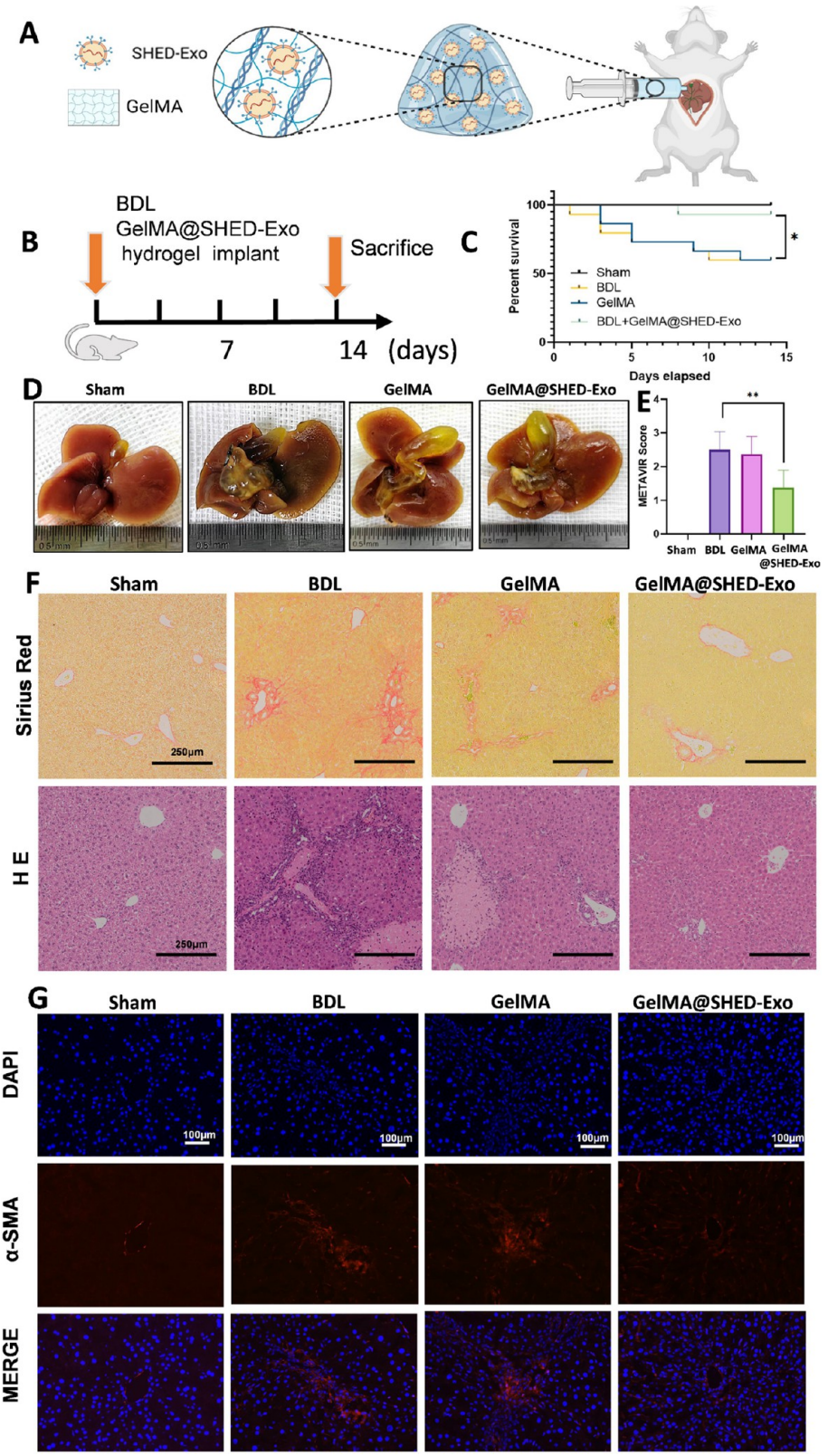

Figure 9. Controlled release of SHED-Exo for liver fibrosis treatment. (A, B) Treatment process schematic (the figure was generated with BioRender). (C) Postoperative survival rate (n = 15). (D) Gross liver morphology. (E, F) Sirius Red and HE staining of liver tissue and METAVIR scoring. (G) Immunofluorescence staining of α-SMA in liver tissue (n = 3; *p < 0.05, **p < 0.01, ***p < 0.001, scale bars: 250 μm, 100 μm).

changes (Figure 9F), indicating effective mitigation of BDL-induced fibrosis. Sirius Red staining, which specifically highlights collagen deposition, demonstrated extensive collagen fiber accumulation around the portal vein in the BDL and GelMA groups with significant peribiliary fibrosis. In contrast, GelMA@SHED-Exo treatment significantly reduced collagen deposition and prevented bridging fibrosis (Figure 9F). Subsequent fibrosis staging confirmed these findings, with

https://doi.org/10.1021/acsami.4c19748
ACS Appl. Mater. Interfaces 2025, 17, 17948−17964

the GelMA@SHED-Exo group displaying intermediate fibrosis levels between the Sham and BDL groups (Figure 9E). Further analysis of α-SMA, a marker of hepatic stellate cell (HSC) activation and fibrosis, showed a substantial decrease in the GelMA@SHED-Exo group, indicating reduced HSC activation and collagen production, thereby ameliorating fibrosis (Figure 9G).

CONCLUSIONS

Exosomes extracted from three distinct MSC sources underwent sRNA sequencing to construct miRNA profiles. The analysis revealed that exosomes from the same MSC source exhibited less interindividual variability compared to those from different tissue origins, with each tissue type showing distinct miRNA enrichment patterns. Additionally, miRNAs enriched in exosomes that regulate macrophage polarization and inflammation were identified. Previous studies have demonstrated that exosome miRNA levels increase proportionally with cell proliferation, allowing for noninvasive, straightforward assessments of cell differentiation via miRNA ratio detection. Thus, these secretome profiles not only provide insights into exosome biology but also offer a potential method for monitoring the cell preparation purity. Given that batch-to-batch variability in exosomes poses a significant challenge for quality control during clinical translation, miRNA profiling presents a viable solution. However, higher-throughput miRNA profiling and further exploration of exosome-mediated regulatory functions in disease models are necessary to establish precise quality control standards.

This study specifically examined the therapeutic potential of SHED-Exo on ALI and its effects on hepatocytes and macrophages. SHED-Exo promoted hepatocyte proliferation and migration, highlighting its potential in liver regeneration and broadening its clinical application while avoiding the tumorigenic risks associated with direct stem cell use. SHED-Exo also modulated macrophage phenotypes, likely linked to miRNAs such as miR-126−5p, miR-142−5p, and let-7b-5p identified in earlier research. Despite these promising findings, several limitations persist. Future research should prioritize the identification of key miRNAs or proteins conveyed by SHED-Exos, especially those implicated in liver injury repair, to discover potential biomarkers. Further exploration is required to elucidate the broader mechanisms of SHED-Exo action in ALI, with a particular focus on interactions with non-parenchymal liver cells. Additionally, given the variability inherent in exosome-based therapies, subsequent studies should aim to establish quality control standards for exosomes by identifying specific biomarkers, thereby ensuring the consistency and reliability of therapeutic outcomes.

Furthermore, a novel injectable GelMA hydrogel loaded with SHED-Exo was developed that exhibits strong adhesion properties suitable for in vivo applications. This hydrogel enabled the sustained release of exosomes, preserving SHED-Exo bioactivity with minimal impact on the properties of GelMA. In vitro, exosomes were released over 14 days, and in vivo retention extended to 28 days. When applied to BDL-induced liver fibrosis, the hydrogel exhibited enhanced therapeutic efficacy without eliciting an immune response. HE staining confirmed the biosafety of GelMA@SHED-Exo. These findings underscore the potential of SHED-Exo-functionalized biomaterials in fibrosis therapy, though limitations remain, such as the need for models representing diverse chronic liver diseases and the elucidation of molecular mechanisms underlying SHED-Exo's antifibrotic effects. Drawing from the findings of this study, subsequent research endeavors will concentrate on standardizing the preparation process for exosome-loaded hydrogels to develop a highly consistent production system. Additionally, the influence of diverse hydrogel materials and carrier systems on therapeutic outcomes will be assessed, with a specific focus on optimizing cross-linking techniques and delivery strategies. Multicenter, multiphase preclinical trials should be undertaken to validate safety and efficacy, as well as to evaluate the therapeutic consistency of exosome-loaded hydrogels across various production batches. These initiatives are intended to bridge the gap between the experimental results and clinical application.

ASSOCIATED CONTENT

Supporting Information

The Supporting Information is available free of charge at https://pubs.acs.org/doi/10.1021/acsami.4c19748.

Primer sequences used for qPCR (PDF)

AUTHOR INFORMATION

Corresponding Authors

Yifan Wang − *Department of General Surgery, Sir Run Run Shaw Hospital, Zhejiang University School of Medicine, Hangzhou 310016, China; National Engineering Research Center of Innovation and Application of Minimally Invasive Instruments, Hangzhou 310016, China; Zhejiang Minimal Invasive Diagnosis and Treatment Technology Research Center of Severe Hepatobiliary Disease, Hangzhou 310016, China;* orcid.org/0000-0002-8828-4268; Email: anwyf@zju.edu.cn

Xiujun Cai − *Department of General Surgery, Sir Run Run Shaw Hospital, Zhejiang University School of Medicine, Hangzhou 310016, China; National Engineering Research Center of Innovation and Application of Minimally Invasive Instruments, Hangzhou 310016, China; Zhejiang Minimal Invasive Diagnosis and Treatment Technology Research Center of Severe Hepatobiliary Disease, Hangzhou 310016, China;* orcid.org/0000-0002-6457-0577; Email: srrsh_cxj@zju.edu.cn

Authors

Ziyuan Wang − *Department of General Surgery, Sir Run Run Shaw Hospital, Zhejiang University School of Medicine, Hangzhou 310016, China*

Danyang Zhong − *Department of General Surgery, Sir Run Run Shaw Hospital, Zhejiang University School of Medicine, Hangzhou 310016, China*

Tingting Yan − *Department of General Surgery, Sir Run Run Shaw Hospital, Zhejiang University School of Medicine, Hangzhou 310016, China*

Qiang Zheng − *Department of General Surgery, Sir Run Run Shaw Hospital, Zhejiang University School of Medicine, Hangzhou 310016, China*

Enjie Zhou − *Department of General Surgery, Sir Run Run Shaw Hospital, Zhejiang University School of Medicine, Hangzhou 310016, China*

Zhichao Ye − *Department of General Surgery, Sir Run Run Shaw Hospital, Zhejiang University School of Medicine, Hangzhou 310016, China*

https://doi.org/10.1021/acsami.4c19748
ACS Appl. Mater. Interfaces 2025, 17, 17948−17964

Xiaoyan He − *Department of General Surgery, Sir Run Run Shaw Hospital, Zhejiang University School of Medicine, Hangzhou 310016, China*
Yu Liu − *Department of Cardiac Surgery, Zhejiang University School of Medicine Sir Run Run Shaw Hospital, Hangzhou 310016 Zhejiang, China*
Jianing Yan − *Department of General Surgery, Sir Run Run Shaw Hospital, Zhejiang University School of Medicine, Hangzhou 310016, China*
Yuyang Yuan − *Department of General Surgery, Sir Run Run Shaw Hospital, Zhejiang University School of Medicine, Hangzhou 310016, China*

Complete contact information is available at: https://pubs.acs.org/10.1021/acsami.4c19748

Author Contributions

#Z.W., D.Z., and T.Y. contributed equally. Z.W., D.Z., and T.Y.: Writing—original draft, methodology, formal analysis, data curation. Q.Z.: Visualization, validation, methodology, formal analysis. E.Z.: Methodology, formal analysis. Z.Y.: Validation, methodology, formal analysis. X.H. and Y.L.: Validation, methodology, formal analysis. J.Y. and Y.Y.: Validation. Y.W.: Writing—review and editing, supervision, project administration, funding acquisition. X.C.: Writing—review and editing, supervision, project administration, conceptualization. All authors read and approved the final manuscript.

Notes

This study received approval from the Ethics Review Committee of Zhejiang University (approval number: ZJU20240031).
All of the authors agree to be published. All of the photos included herein were taken by the authors, and the TOC graphic is an original creation by the authors.
The authors declare no competing financial interest.

■ ACKNOWLEDGMENTS

This work was supported by the National Natural Science Foundation of China (Grant No. 82170616) and the Major Program of Natural Science Foundation of Zhejiang Province, China (Grant No. LHDMD23H030001). Some elements of the figures and Table of Contents (TOC) graphic in this article are from biorender.com and Figdraw.com.

■ ABBREVIATIONS

ALI, acute liver injury
SHED, human-derived exfoliated deciduous mesenchymal stem cells
SHED-Exo, SHED cell-derived exosomes
CCl4, carbon tetrachloride
MSCs, mesenchymal stem cells
BMSCs, bone marrow mesenchymal stem cells
UC-MSC, umbilical cord-derived MSCs
H&E, hematoxylin and eosin
IHC, immunohistochemical
TAA, thioacetamide
LPS, lipopolysaccharide
IL-4, interleukin-4
ALT, alanine aminotransferase
AST, aspartate aminotransferase
BDL, bile duct ligation

■ REFERENCES

(1) Shiels, M. S.; Chernyavskiy, P.; Anderson, W. F.; Best, A. F.; Haozous, E. A.; Hartge, P.; Rosenberg, P. S.; Thomas, D.; Freedman, N. D.; Berrington de Gonzalez, A. Trends in premature mortality in the USA by sex, race, and ethnicity from 1999 to 2014: an analysis of death certificate data. *Lancet* **2017**, *389* (10073), 1043−1054.
(2) Williams, R.; Alexander, G.; Aspinall, R.; Bosanquet, J.; Camps-Walsh, G.; Cramp, M.; Day, N.; Dhawan, A.; Dillon, J.; Dyson, J.; et al. New metrics for the Lancet Standing Commission on Liver Disease in the UK. *Lancet (London, England)* **2017**, *389* (10083), 2053−2080.
(3) Tsiapalis, D.; O'Driscoll, L. Mesenchymal Stem Cell Derived Extracellular Vesicles for Tissue Engineering and Regenerative Medicine Applications. *Cells* **2020**, *9* (4), 991.
(4) Kwon, S. G.; Kwon, Y. W.; Lee, T. W.; Park, G. T.; Kim, J. H. Recent advances in stem cell therapeutics and tissue engineering strategies. *Biomaterials research* **2018**, *22*, 36−36.
(5) Wagner, W.; Wein, F.; Seckinger, A.; Frankhauser, M.; Wirkner, U.; Krause, U.; Blake, J.; Schwager, C.; Eckstein, V.; Ansorge, W.; et al. Comparative characteristics of mesenchymal stem cells from human bone marrow, adipose tissue, and umbilical cord blood. *Experimental Hematology* **2005**, *33* (11), 1402−1416.
(6) Hass, R.; Kasper, C.; Boehm, S.; Jacobs, R. Different populations and sources of human mesenchymal stem cells (MSC): A comparison of adult and neonatal tissue-derived MSC. *Cell Commun. Signal.* **2011**, *9*, 12.
(7) Musial-Wysocka, A.; Kot, M.; Majka, M. The Pros and Cons of Mesenchymal Stem Cell-Based Therapies. *Cell Transplantation* **2019**, *28* (7), 801−812.
(8) Egusa, H.; Sonoyama, W.; Nishimura, M.; Atsuta, I.; Akiyama, K. Stem cells in dentistry–part I: stem cell sources. *J. Prosthodont Res.* **2012**, *56* (3), 151−165.
(9) Magalhães, F. D.; Sarra, G.; Carvalho, G. L.; Pedroni, A. C. F.; Marques, M. M.; Chambrone, L.; Gimenez, T.; Moreira, M. S. Dental tissue-derived stem cell sheet biotechnology for periodontal tissue regeneration: A systematic review. *Arch Oral Biol.* **2021**, *129*, No. 105182.
(10) Mosaddad, S. A.; Rasoolzade, B.; Namanloo, R. A.; Azarpira, N.; Dortaj, H. Stem cells and common biomaterials in dentistry: a review study. *Journal of materials science. Materials in medicine* **2022**, *33* (7), 55.
(11) Botelho, J.; Cavacas, M. A.; Machado, V.; Mendes, J. J. Dental stem cells: recent progresses in tissue engineering and regenerative medicine. *Ann. Med.* **2017**, *49* (8), 644−651.
(12) Du, Z.-H.; Chu, W.-X.; Peng, X.; Wu, L.-L.; Liu, Y.; Yu, G.-Y.; Ding, C. SHED-Derived Exosomes Ameliorate Sjögren's Syndrome-Induced Hyposalivation by Suppressing Th1 Cell Response via the miR-29a-3p/T-bet Axis. *ACS Appl. Mater. Interfaces* **2025**, *17* (4), 5752−5761.
(13) Jin, S.; Wang, Y.; Wu, X.; Li, Z.; Zhu, L.; Niu, Y.; Zhou, Y.; Liu, Y. Young Exosome Bio-Nanoparticles Restore Aging-Impaired Tendon Stem/Progenitor Cell Function and Reparative Capacity. *Adv. Mater.* **2023**, *35* (18), No. e2211602.
(14) Liu, P.; Zhang, Q.; Mi, J.; Wang, S.; Xu, Q.; Zhuang, D.; Chen, W.; Liu, C.; Zhang, L.; Guo, J.; et al. Exosomes derived from stem cells of human deciduous exfoliated teeth inhibit angiogenesis in vivo and in vitro via the transfer of miR-100−5p and miR-1246. *Stem Cell Res. Ther* **2022**, *13* (1), 89.
(15) Liu, Y.; Jing, H.; Kou, X.; Chen, C.; Liu, D.; Jin, Y.; Lu, L.; Shi, S. PD-1 is required to maintain stem cell properties in human dental pulp stem cells. *Cell Death Differ.* **2018**, *25* (7), 1350−1360.
(16) Bernal, W.; Wendon, J. Acute liver failure. *N Engl J. Med.* **2013**, *369* (26), 2525−2534.
(17) Margiana, R.; Markov, A.; Zekiy, A. O.; Hamza, M. U.; Al-Dabbagh, K. A.; Al-Zubaidi, S. H.; Hameed, N. M.; Ahmad, I.; Sivaraman, R.; Kzar, H. H.; et al. Clinical application of mesenchymal stem cell in regenerative medicine: a narrative review. *Stem Cell Res. Ther* **2022**, *13* (1), 366.

(18) Hu, C.; Zhao, L.; Zhang, L.; Bao, Q.; Li, L. Mesenchymal stem cell-based cell-free strategies: safe and effective treatments for liver injury. *Stem Cell Res. Ther* **2020**, *11* (1), 377.
(19) Liu, J.; Song, J.; Yuan, H.; Li, X.; Li, N.; Duan, L. Biogenic matter characteristics, deposition flux correction, and internal phosphorus transformation in Jiaozhou Bay, North China. *Journal of Marine Systems* **2019**, *196*, 1−13.
(20) Kalluri, R.; LeBleu, V. S. The biology, function, and biomedical applications of exosomes. *Science* **2020**, *367* (6478), No. eaau6977.
(21) Ahmed, T.; Ahmad, J. Recent advances in the diagnosis of drug-induced liver injury. *World J. Hepatol* **2024**, *16* (2), 186−192.
(22) Shao, M.; Xu, Q.; Wu, Z.; Chen, Y.; Shu, Y.; Cao, X.; Chen, M.; Zhang, B.; Zhou, Y.; Yao, R.; et al. Exosomes derived from human umbilical cord mesenchymal stem cells ameliorate IL-6-induced acute liver injury through miR-455−3p. *Stem Cell Res. Ther* **2020**, *11* (1), 37.
(23) Masako Miura, S. G.; Zhao, M.; Lu, B.; Fisher, L. W.; Robey, P. G.; Shi, S. SHED: stem cells from human exfoliated deciduous teeth. *Proc. Natl. Acad. Sci. U. S. A.* **2003**, *100* (10), 5807−5812.
(24) Muto, H.; Ito, T.; Tanaka, T.; Yokoyama, S.; Yamamoto, K.; Imai, N.; Ishizu, Y.; Maeda, K.; Honda, T.; Ishikawa, T.; et al. Conditioned medium from stem cells derived from human exfoliated deciduous teeth ameliorates NASH via the Gut-Liver axis. *Sci. Rep* **2021**, *11* (1), 18778.
(25) Sonoda, S.; Murata, S.; Yamaza, H.; Yuniartha, R.; Fujiyoshi, J.; Yoshimaru, K.; Matsuura, T.; Oda, Y.; Ohga, S.; Tajiri, T.; et al. Targeting hepatic oxidative stress rescues bone loss in liver fibrosis. *Mol. Metab* **2022**, *66*, No. 101599.
(26) Matsushita, Y.; Ishigami, M.; Matsubara, K.; Kondo, M.; Wakayama, H.; Goto, H.; Ueda, M.; Yamamoto, A. Multifaceted therapeutic benefits of factors derived from stem cells from human exfoliated deciduous teeth for acute liver failure in rats. *J. Tissue Eng. Regen Med.* **2017**, *11* (6), 1888−1896.
(27) Hirata, M.; Ishigami, M.; Matsushita, Y.; Ito, T.; Hattori, H.; Hibi, H.; Goto, H.; Ueda, M.; Yamamoto, A. Multifaceted Therapeutic Benefits of Factors Derived From Dental Pulp Stem Cells for Mouse Liver Fibrosis. *Stem Cells Transl Med.* **2016**, *5* (10), 1416−1424.
(28) Zhang, Q.; Liu, L. N.; Yong, Q.; Deng, J. C.; Cao, W. G. Intralesional injection of adipose-derived stem cells reduces hypertrophic scarring in a rabbit ear model. *Stem Cell Res. Ther* **2015**, *6* (1), 145.
(29) Zhang, W.; Ling, Q.; Wang, B.; Wang, K.; Pang, J.; Lu, J.; Bi, Y.; Zhu, D. Comparison of therapeutic effects of mesenchymal stem cells from umbilical cord and bone marrow in the treatment of type 1 diabetes. *Stem Cell Res. Ther* **2022**, *13* (1), 406.
(30) He, X.; Wang, L.; Liu, L.; Gao, J.; Long, B.; Chi, F.; Hu, T.; Wan, Y.; Gong, Z.; Li, L.; et al. Endogenous alpha7 nAChR Agonist SLURP1 Facilitates Escherichia coli K1 Crossing the Blood-Brain Barrier. *Front Immunol* **2021**, *12*, No. 745854.
(31) Liu, M.; Lu, J.; Hu, J.; Chen, Y.; Deng, X.; Wang, J.; Zhang, S.; Guo, J.; Li, W.; Guan, S. Sodium sulfite triggered hepatic apoptosis, necroptosis, and pyroptosis by inducing mitochondrial damage in mice and AML-12 cells. *J. Hazard Mater.* **2024**, *467*, No. 133719.
(32) Chen, X.; He, F.; Zhong, D. Y.; Luo, Z. P. Acoustic-frequency vibratory stimulation regulates the balance between osteogenesis and adipogenesis of human bone marrow-derived mesenchymal stem cells. *Biomed. Res. Int.* **2015**, *2015*, No. 540731.
(33) Li, P.; Kaslan, M.; Lee, S. H.; Yao, J.; Gao, Z. Progress in Exosome Isolation Techniques. *Theranostics* **2017**, *7* (3), 789−804.
(34) Siegel, G.; Kluba, T.; Hermanutz-Klein, U.; Bieback, K.; Northoff, H.; Schäfer, R. Phenotype, donor age and gender affect function of human bone marrow-derived mesenchymal stromal cells. *BMC Med.* **2013**, *11*, 146.
(35) Kowal, J. M.; Möller, S.; Ali, D.; Figeac, F.; Barington, T.; Schmal, H.; Kassem, M. Identification of a clinical signature predictive of differentiation fate of human bone marrow stromal cells. *Stem Cell Res. Ther* **2021**, *12* (1), 265.
(36) Harrell, C. R.; Fellabaum, C.; Jovicic, N.; Djonov, V.; Arsenijevic, N.; Volarevic, V. Molecular Mechanisms Responsible for Therapeutic Potential of Mesenchymal Stem Cell-Derived secretome. *Cells* **2019**, *8* (5), 467.
(37) Bastidas, J. G.; Maurmann, N.; Scholl, J. N.; Weber, A. F.; Silveira, R. P.; Figueiro, F.; Stimamiglio, M. A.; Marcon, B.; Correa, A.; Pranke, P. secretome of stem cells from human exfoliated deciduous teeth (SHED) and its extracellular vesicles improves keratinocytes migration, viability, and attenuation of H(2) O(2) -induced cytotoxicity. *Wound Repair Regen* **2023**, *31* (6), 827−841.
(38) Chandy, M.; Rhee, J.-W.; Ozen, M. O.; Williams, D. R.; Pepic, L.; Liu, C.; Zhang, H.; Malisa, J.; Lau, E.; Demirci, U.; et al. Atlas of exosomal microRNAs Secreted From Human iPSC-Derived Cardiac Cell Types. *Circulation* **2020**, *142* (18), 1794−1796.
(39) Jiang, J.; Xin, J.; Ding, W.; Shi, D.; Sun, S.; Guo, B.; Zhou, X.; Zheng, C.; Li, J. MicroRNA Profile of Human Bone Marrow Mesenchymal Stem Cells during Hepatic Differentiation and Therapy. *Int. J. Med. Sci.* **2022**, *19* (1), 152−163.
(40) Squadrito, M. L.; Etzrodt, M.; De Palma, M.; Pittet, M. J. MicroRNA-mediated control of macrophages and its implications for cancer. *Trends Immunol* **2013**, *34* (7), 350−359.
(41) Ghafouri-Fard, S.; Abak, A.; Tavakkoli Avval, S.; Shoorei, H.; Taheri, M.; Samadian, M. The impact of non-coding RNAs on macrophage polarization. *Biomed Pharmacother* **2021**, *142*, No. 112112.
(42) Gu, W.; Yao, L.; Li, L.; Zhang, J.; Place, A. T.; Minshall, R. D.; Liu, G. ICAM-1 regulates macrophage polarization by suppressing MCP-1 expression via miR-124 upregulation. *Oncotarget* **2017**, *8* (67), 111882−111901.
(43) Wang, J.; Tian, F.; Cao, L.; Du, R.; Tong, J.; Ding, X.; Yuan, Y.; Wang, C. Macrophage polarization in spinal cord injury repair and the possible role of microRNAs: A review. *Heliyon* **2023**, *9* (12), No. e22914.
(44) Lazaro-Ibanez, E.; Faruqu, F. N.; Saleh, A. F.; Silva, A. M.; Tzu-Wen Wang, J.; Rak, J.; Al-Jamal, K. T.; Dekker, N. Selection of Fluorescent, Bioluminescent, and Radioactive Tracers to Accurately Reflect Extracellular Vesicle Biodistribution in Vivo. *ACS Nano* **2021**, *15* (2), 3212−3227.
(45) Zhou, J.; Feng, X.; Zhu, J.; Feng, B.; Yao, Q.; Pan, Q.; Yu, J.; Yang, J.; Li, L.; Cao, H. Mesenchymal stem cell treatment restores liver macrophages homeostasis to alleviate mouse acute liver injury revealed by single-cell analysis. *Pharmacological research* **2022**, *179*, No. 106229.
(46) Slautin, V.; Konyshev, K.; Gavrilov, I.; Beresneva, O.; Maklakova, I.; Grebnev, D. Fucoxanthin Enhances the Antifibrotic Potential of Placenta-derived Mesenchymal Stem Cells in a CCl4-induced Mouse Model of Liver Fibrosis. *Curr. Stem Cell Res. Ther* **2024**, *19* (11), 1484−1496.
(47) Guilliams, M.; Scott, C. L. Liver macrophages in health and disease. *Immunity* **2022**, *55* (9), 1515−1529.
(48) Murray, P. J.; Wynn, T. A. Protective and pathogenic functions of macrophage subsets. *Nat. Rev. Immunol* **2011**, *11* (11), 723−737.
(49) Triantafyllou, E.; Woollard, K. J.; McPhail, M. J. W.; Antoniades, C. G.; Possamai, L. A. The Role of Monocytes and Macrophages in Acute and Acute-on-Chronic Liver Failure. *Front Immunol* **2018**, *9*, 2948.
(50) Wei, H.; Wu, X.; Huang, L.; Long, C.; Lu, Q.; Huang, Z.; Huang, Y.; Li, W.; Pu, J. LncRNA MEG3 Reduces the Ratio of M2/M1Macrophages Through the HuR/CCL5 Axis in Hepatocellular Carcinoma. *J. Hepatocell Carcinoma* **2024**, *11*, 543−562.
(51) Zhao, J.; Feng, Y.; Liu, X.; Li, H.; Guo, H.; Ke, J.; Long, X. The relationship of ALPK1, hyaluronic acid and M1 macrophage polarization in the temporomandibular joint synovitis. *J. Cell Mol. Med.* **2024**, *28* (7), No. e18172.
(52) Deng, Y.; Li, Y.; Chu, Z.; Dai, C.; Ge, J. Exosomes from umbilical cord-derived mesenchymal stem cells combined with gelatin methacryloyl inhibit vein graft restenosis by enhancing endothelial functions. *J. Nanobiotechnol.* **2023**, *21* (1), 380.

https://doi.org/10.1021/acsami.4c19748
ACS Appl. Mater. Interfaces 2025, 17, 17948−17964